Available online at www.sciencedirect.com
ScienceDirect
Journal of Sound and Vibration 315 (2008) 318–342
JOURNAL OF SOUND AND VIBRATION
www.elsevier.com/locate/jsvi

Exact solution for linear buckling of rectangular Mindlin plates

Shahrokh Hosseini-Hashemi[a], Korosh Khorshidi[a,*], Marco Amabili[b]

[a]*Department of Mechanical Engineering, Iran University of Science and Technology, Narmak, Tehran 16846-13114, Iran*
[b]*Dipartimento di Ingegneria Industriale, Università di Parma, Parco Area delle Scienze 181/A, Parma 43100, Italy*

Received 6 July 2007; received in revised form 31 January 2008; accepted 31 January 2008
Handling Editor: A.V. Metrikine
Available online 14 March 2008

Abstract

In the present paper, the Mindlin plate theory is used to study buckling of in-plane loaded isotropic rectangular plates with different boundary conditions. The novelty of the paper is that the analytical closed-form solution is developed without any use of approximation for a combination of six different boundary conditions; specifically, two opposite edges are simply supported and any of the other two edges can be simply supported, clamped or free. Monoaxial in-plane compressive loads on both directions are considered, as well as equal biaxial loads. The present analytical solution can be obtained with any required accuracy and can be used as benchmark. Dimensionless critical buckling loads and mode shapes are given for the six cases analyzed. The effect of boundary conditions, loading conditions, variations of aspect ratios and thickness ratios are examined and discussed in detail. Finally, based on comparison with previously published results, the accuracy of the results is shown.

1. Introduction

Thick plates are important structural elements and are widely used in engineering applications. They can be analyzed by using the classical Kirchhoff thin plate theory, but, because the effects of transverse shear deformation are neglected, the deflections are underestimated and the natural frequencies and buckling loads are overestimated.

In order to deal with thicker and laminated composite plates, the Mindlin theory of plates (first-order shear deformation theory) was introduced to take into account transverse shear strains. Five variables are used in this theory to describe the deformation: three displacements of the middle surface and two rotations. In case of flat plates (without geometric imperfections), the in-plane displacements are uncoupled from the transverse displacement and rotations.

The Mindlin approach [1] does not satisfy the transverse shear boundary conditions at the top and bottom surfaces of the plate, since a constant shear angle through the thickness is assumed, and plane sections remain plane after deformation. As a consequence of this approximation, the Mindlin theory of plates requires shear correction factors for equilibrium considerations. For this reason, Reddy [1,2] has developed a nonlinear plate

*Corresponding author. Tel.: +98 21 7391 2912; fax: +98 21 7724 0488.
E-mail address: k_khorshidi@iust.ac.ir (K. Khorshidi).

0022-460X/$ - see front matter © 2008 Elsevier Ltd. All rights reserved.
doi:10.1016/j.jsv.2008.01.059

theory that includes cubic terms (in the distance from the middle surface of the plate) in the in-plane displacement kinematics. This higher-order shear deformation theory satisfies zero transverse shear stresses at the top and bottom surfaces of the plate; up to cubic terms are retained, giving a parabolic shear strain distribution through the thickness, resembling with good approximation the results of three-dimensional elasticity; therefore, shear correction factors are not required.

A synthetic literature review is presented here. Extensive analyses for elastic stability of rectangular plates of both constant and variable thickness on the basis of the classical Kirchhoff plate theory have been carried out by using exact and numerical methods, and a considerable amount of information on the buckling loads for different boundary conditions and in-plane loadings is available in the literature (e.g., see Refs. [3–5]). On the other hand, the literature on elastic buckling of moderately thick plates based on Mindlin and third-order shear deformation theories, is not so extensive (e.g., see Ref. [6]). Srinivas [7] presented an exact three-dimensional elastic analysis for the stability of thick simply supported rectangular plates. Brunelle [8] analyzed the elastic buckling of transversely isotropic Mindlin plates with two parallel edges simply supported and the remaining two edges subjected to a variety of boundary conditions. Brunelle and Robertson [9] derived the governing equations of a transversely isotropic, initially stressed Mindlin plate, and solved the thick plate equations for simply supported rectangular plates in a state of uniform compressive stress plus a uniform bending stress both acting in the same direction. Rao et al. [10] analyzed the stability of moderately thick rectangular plates by using a triangular finite element. Luo [11] presented the finite element analysis for the buckling of thin and moderately thick plates by means of a modified complementary energy principle, and showed the simplicity and reliability of the method. Sakiyama and Matsuda [12] analyzed the elastic buckling of rectangular Mindlin plates with mixed boundary conditions using integral equations combined with a numerical integration technique.

Wang [13] obtained a relationship between the elastic buckling loads of classical Kirchhoff plates and Mindlin plates. Wang and Reddy [14] presented an analogous relationship between the elastic buckling loads of Kirchhoff and third-order shear deformation polygonal plates with simply supported edges.

Leissa and Kang using the classical power series method to get the exact solutions for free vibration and buckling of S-C-S-C [15] and S-F-S-F [16] (SS, simply supported edge; C, clamped edge; F, free edge) thin plates loaded at the simply supported edges by linearly varying in-plane distributed forces and moments. Kang and Leissa [17] extended their analysis to buckling of rectangular thin plates having two opposite edges simply supported and subjected to linearly varying in-plane load. Reddy and Phan [18] obtained exact buckling loads and natural frequencies of simply supported rectangular plates by using a higher-order shear deformation theory.

Liew et al. [19] calculated the buckling loads of rectangular Mindlin plates having two parallel edges simply supported, one edge free and the remaining edge with free, simply supported or clamped boundary condition. Wang et al. [20] presented general buckling solutions for in-plane loaded, isotropic Mindlin plates of rectangular, polygonal, elliptical, semicircular and annular shape. Liew et al. [21], by using the differential quadrature method, studied buckling behavior of rectangular plates resting on Winkler foundation based an approximate analysis and the Mindlin plate theory. Shen studied the postbuckling of rectangular Mindlin plates with four simply supported edges [22], and four free edges [23], subjected to biaxial compression combined with lateral pressure and resting on a two-parameter (Pasternak-type) elastic foundation. In his work, the initial geometrical imperfection of the plate was also taken into account. Mizusawa [24] applied the spline strip method to compute the buckling load parameters of rectangular thick, uniform and tapered, plates under uniform in-plane loads with a few different boundary conditions. The canonical exact solutions for elastic bending, buckling and free vibration of plates resting on two-parameter foundations were obtained by Lam et al. [25] by using Green's functions. Penga et al. [26] presented a mesh-free Galerkin method for free vibration and stability analysis of stiffened Mindlin plates.

The first analytical solutions for buckling and free vibration of stepped rectangular Mindlin plates with two opposite edges simply supported and the remaining two edges being free, simply supported or clamped was obtained by Xiang and Wei [27].

The Rayleight–Ritz method and the finite strip method were used by Dawe and Roupaeil [28] to study elastic buckling of rectangular Mindlin plates. Xiang [29] studied buckling and free vibrations of Mindlin plates by using the Rayleigh–Ritz method; the same approach was used by Kitipornchai et al. [30] to analyze

skew plates; skew plates on Pasternak foundation were investigated by Xiang et al. [31,32]. Wang et al. [33] considered the elastic buckling of rectangular Mindlin plates with internal line supports.

Liew and Chen [34] considered elastic buckling of rectangular Mindlin plates subjected to partially distributed in-plane loads by using the radial point interpolation method. Shufrin and Eisenberger [35] analyzed the stability and vibration of the shear deformable first-order (Mindlin) and higher-order (Reddy) plates by using the extended Kantorovich method. Liu [36] investigated buckling of discontinuous (cracked) rectangular Mindlin plates.

In the present paper, the Mindlin plate theory is used to study buckling of in-plane loaded isotropic rectangular plates with different boundary conditions. The novelty of the paper is that the analytical closed-form solution is developed without any use of approximation for a combination of six different boundary conditions; specifically, two opposite edges are simply supported and any of the other two edges can be simply supported, clamped or free. Monoaxial in-plane compressive loads on both directions are considered, as well as equal biaxial loads. The present solution is an extension of the free vibration analysis developed by Hosseini-Hashemi and Arsanjani [38] for unloaded, rectangular Mindlin plates. The present analytical solution can be obtained with any required accuracy and can be used as a benchmark.

2. Governing equations and their dimensionless forms

Consider a flat, isotropic, rectangular Mindlin plate of uniform thickness h, length a, width b, modulus of elasticity E, Poisson's ratio v, shear modulus $G = E/2(1+v)$ and mass per unit volume ρ, oriented so that its mid-plane surface contains the x_1 and x_2-axis of a Cartesian coordinate system (x_1,x_2,x_3). The plate is subjected to in-plane edge loads per unit length N_1 in the x_1 direction and N_2 in the x_2 direction, as shown in Fig. 1. The two edges of the plate parallel to the x_2-axis are assumed to be simply supported while the other two edges may have any combinations of clamped, free or simply supported boundary conditions as shown in Fig. 2.

It is not difficult to show that the resultant force due to components of the in-plane edge loads in transverse direction for a deflected plate is

$$p_1 = N_1\psi_{3,11} + N_2\psi_{3,22}, \tag{1}$$

where ψ_3 is the plate transverse deflection and p_1 is the force per unit area positive in x_3 direction. In Eq. (1) and in the following part of the present paper, the symbol "," is used to indicate derivative; e.g. $\psi_{3,11}$ is equivalent to $\partial^2\psi_3/\partial^2 x_1$ while $\psi_{3,1}$ is simply $\partial\psi_3/\partial x_1$.

The governing differential equations based on the Mindlin first-order shear deformation plate theory in absence of in-plane stress resultants are given by [38]

$$M_{11,1} + M_{12,2} - Q_1 = -\frac{1}{12}\rho h^3\ddot{\psi}_1, \tag{2a}$$

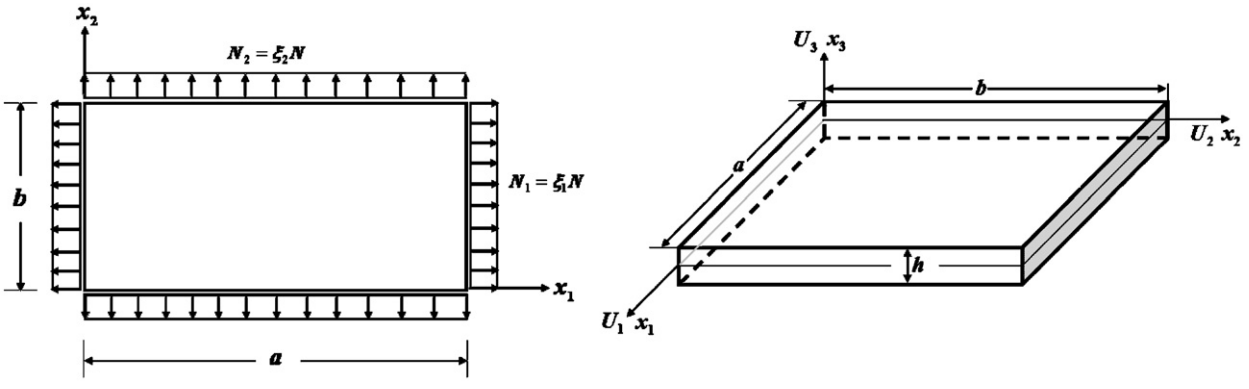

Fig. 1. A rectangular Mindlin plate subjected to in-plane edge loads.

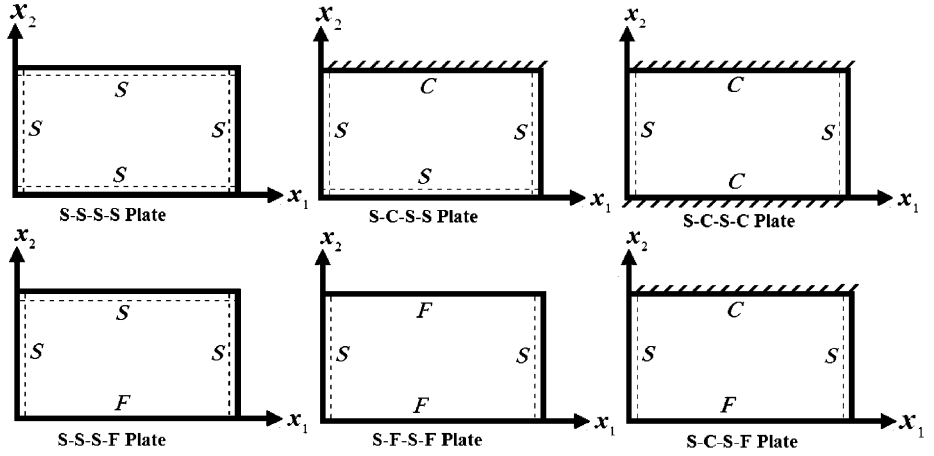

Fig. 2. Boundary conditions of the Mindlin plates analyzed.

$$M_{12,1} + M_{22,2} - Q_2 = -\frac{1}{12}\rho h^3 \ddot{\psi}_2, \tag{2b}$$

$$Q_{1,1} + Q_{2,2} + p = \rho h \ddot{\psi}_3, \tag{2c}$$

where ψ_1 and ψ_2 are the rotations of the transverses normal about the x_2- and x_1-axis, respectively, M_{11} and M_{22} are the bending moments, M_{12} is the twisting moment, and Q_1 and Q_2 are the transverse shear forces. The stress resultants are

$$M_{11} = -D(\psi_{1,1} + \nu\psi_{2,2}), \quad M_{22} = -D(\psi_{2,2} + \nu\psi_{1,1}), \tag{3a,b}$$

$$M_{12} = -\frac{D}{2}(1-\nu)(\psi_{1,2} + \psi_{2,1}), \tag{3c}$$

$$Q_1 = -\kappa^2 Gh(\psi_1 - \psi_{3,1}), \quad Q_2 = -\kappa^2 Gh(\psi_2 - \psi_{3,2}), \tag{3d,e}$$

where $D = Eh^3/(12(1-\nu^2))$ is the flexural rigidity and κ^2 is the shear correction factor since the transverse shear strains are not truly independent of the thickness coordinate but nearly parabolic.

In order to derive the governing differential equations for the plate under consideration, the transverse force p in Eq. (2c) may be interpreted as

$$p = p_2 + p_1 = N_1\psi_{3,11} + N_2\psi_{3,22} + p_2, \tag{4}$$

where p_2 is any applied transverse distributed load or point loads opposing the x_3-direction. In absence of the applied load p_2 and assuming free harmonic motion, the governing differential equations for free vibration of the plate under investigation may be presented in terms of ψ_1, ψ_2 and ψ_3 by substituting the stress resultants from expressions (3a–e) and Eq. (4) into Eqs. (2a–c). Thus we obtain

$$D[\nu_1(\overline{\psi}_{1,11} + \overline{\psi}_{1,22}) + \nu_2(\overline{\psi}_{1,11} + \overline{\psi}_{2,12}) - \kappa^2 Gh(\overline{\psi}_1 - \overline{\psi}_{3,1})] = -\frac{1}{12}\rho h^3\omega^2\overline{\psi}_1, \tag{5a}$$

$$D[\nu_1(\overline{\psi}_{2,11} + \overline{\psi}_{2,22}) + \nu_2(\overline{\psi}_{1,12} + \overline{\psi}_{2,22}) - \kappa^2 Gh(\overline{\psi}_2 - \overline{\psi}_{3,2})] = -\frac{1}{12}\rho h^3\omega^2\overline{\psi}_2, \tag{5b}$$

$$\kappa^2 Gh(\overline{\psi}_{3,11} + \overline{\psi}_{3,22} - \overline{\psi}_{1,1} - \overline{\psi}_{2,2}) + N_1\overline{\psi}_{3,11} + N_2\overline{\psi}_{3,22} = -\rho h\omega^2\overline{\psi}_3, \tag{5c}$$

where ω is the free vibration frequency of the plate

$$\psi_1(x_1, x_2, t) = \overline{\psi}_1(x_1, x_2)\,\mathrm{e}^{-\mathrm{i}\omega t}, \quad \psi_2(x_1, x_2, t) = \overline{\psi}_2(x_1, x_2)\,\mathrm{e}^{-\mathrm{i}\omega t}, \tag{6a,b}$$

$$\psi_3(x_1,x_2,t)=\overline{\psi}_3(x_1,x_2)\,\mathrm{e}^{-\mathrm{i}\omega t},\quad v_1=\frac{1-v}{2},\quad v_2=\frac{1+v}{2}. \tag{6c–e}$$

For generality and convenience, the coordinates are normalized with respect to the plate planar dimensions and the following nondimensional terms are introduced:

$$\begin{aligned}
&X_1=\frac{x_1}{a},\quad X_2=\frac{x_2}{a},\quad \delta=\frac{h}{a},\quad \eta=\frac{a}{b},\quad (\tilde{\psi}_1,\tilde{\psi}_2)=(\overline{\psi}_1,\overline{\psi}_2),\quad \tilde{\psi}_3=\frac{\overline{\psi}_3}{a},\\
&(\tilde{M}_{11},\tilde{M}_{22},\tilde{M}_{12})=(M_{11},M_{22},M_{12})\frac{a}{D},\quad (\tilde{Q}_1,\tilde{Q}_2)=\frac{(Q_1,Q_2)}{\kappa^2 Gh},\\
&(\tilde{N}_1,\tilde{N}_2)=(N_1,N_2)\frac{a^2}{D},\quad \beta=\omega a^2\sqrt{\frac{\rho h}{D}},\quad \theta=12\frac{\kappa^2 v_1}{\delta^2},
\end{aligned} \tag{7}$$

where β is the frequency parameter. Introducing dimensionless terms, also enables Eqs. (5a–c) to be written in dimensionless form as

$$\tilde{\psi}_{1,11}+\eta^2\tilde{\psi}_{1,22}+\frac{v_2}{v_1}(\tilde{\psi}_{1,11}+\eta\tilde{\psi}_{2,12})-\frac{\theta}{v_1}(\tilde{\psi}_1-\tilde{\psi}_{3,1})=-\frac{\kappa^2}{\theta}\beta^2\tilde{\psi}_1, \tag{8a}$$

$$\tilde{\psi}_{2,11}+\eta^2\tilde{\psi}_{2,22}+\frac{v_2}{v_1}\eta(\tilde{\psi}_{1,12}+\eta\tilde{\psi}_{2,22})-\frac{\theta}{v_1}(\tilde{\psi}_2-\eta\tilde{\psi}_{3,2})=-\frac{\kappa^2}{\theta}\beta^2\tilde{\psi}_2, \tag{8b}$$

$$(\theta+\tilde{N}_1)\tilde{\psi}_{3,11}+(\theta+\tilde{N}_2)\eta^2\tilde{\psi}_{3,22}-\theta(\tilde{\psi}_{1,1}+\tilde{\psi}_{2,2})=-\beta^2\tilde{\psi}_3. \tag{8c}$$

The boundary conditions to be applied to the dimensionless equations for an edge parallel to the X_1-normalized axis ($X_2=0$ or $X_2=1$) are given by

$$\tilde{M}_{22}=0,\quad \tilde{\psi}_1=0,\quad \tilde{\psi}_3=0\quad \text{for a simply supported edge,} \tag{9a–c}$$

$$\tilde{M}_{22}=0,\quad \tilde{M}_{12}=0,\quad \tilde{Q}_2+\frac{\eta}{\theta}\tilde{N}_2\tilde{\psi}_{3,2}=0\quad \text{for a free edge,} \tag{10a–c}$$

$$\tilde{\psi}_1=0,\quad \tilde{\psi}_2=0,\quad \tilde{\psi}_3=0\quad \text{for a clamped edge.} \tag{11a–c}$$

The corresponding boundary conditions for the simply supported edge at both $X_1=0$ and $X_1=1$ are obtained by interchanging subscripts 1 and 2 in Eqs. (9a–c).

The three dimensionless governing Eqs. (8a–c) may be solved (see Appendix A for details) by representing the three dimensionless functions $\tilde{\psi}_1$, $\tilde{\psi}_2$ and $\tilde{\psi}_3$ in terms of the three dimensionless potentials W_1, W_2 and W_3 as [37,38]

$$\tilde{\psi}_1=C_1W_{1,1}+C_2W_{2,1}-\eta W_{3,2},\quad \tilde{\psi}_2=C_1\eta W_{1,2}+C_2\eta W_{2,2}+W_{3,1}, \tag{12a,b}$$

$$\tilde{\psi}_3=W_1+W_2, \tag{12c}$$

where W_1, W_2 and W_3 are characterized by the equations,

$$W_{1,11}+\eta^2W_{1,22}=-\alpha_1^2W_1,\quad W_{2,11}+\eta^2W_{2,22}=-\alpha_2^2W_2,\quad W_{3,11}+\eta^2W_{3,22}=-\alpha_3^2W_3, \tag{13a–c}$$

and C_1, C_2, α_1, α_2 and α_3 are coefficients to be determined.

For the plate with simply supported edges at both $X_1=0$ and $X_1=1$, one set of solutions to Eqs. (13a–c) may be given by

$$W_1=[A_1\sin(\lambda_1X_2)+A_2\cos(\lambda_1X_2)]\sin(\mu X_1), \tag{14a}$$

$$W_2=[A_3\sinh(\lambda_2X_2)+A_4\cosh(\lambda_2X_2)]\sin(\mu X_1), \tag{14b}$$

$$W_3=[A_5\sinh(\lambda_3X_2)+A_6\cosh(\lambda_3X_2)]\cos(\mu X_1), \tag{14c}$$

where $\mu=m\pi$; $m=1,2,\ldots$ and A_i are the arbitrary constants. λ_i and μ are also related to the α_i by

$$\alpha_1^2=\mu^2+\eta^2\lambda_1^2,\quad \alpha_2^2=\mu^2-\eta^2\lambda_2^2,\quad \alpha_3^2=\mu^2-\eta^2\lambda_3^2. \tag{15a–c}$$

The details of existence of the other sets of solutions of Eqs. (13a–c) are given in Appendix B. It should be emphasized that, as shown in Appendix B, the set of solutions given in Eqs. (14a–c) are based on the assumption that $\alpha_1^2>0$, $\alpha_2^2<0$, $\alpha_3^2<0$.

As shown in Appendix A, the coefficients λ_1, λ_2 and α_3 are expressed as

$$\lambda_1^2=\frac{-\lambda+\sqrt{\lambda^2-4\alpha}}{2},\quad \lambda_2^2=\frac{\lambda+\sqrt{\lambda^2-4\alpha}}{2},\quad \alpha_3^2=\frac{12\kappa^2}{\beta^2\delta^2}\alpha_1^2\alpha_2^2=\frac{\kappa^2\beta^2}{\theta}-\frac{\theta}{\nu_1},$$
$$\lambda_3^2=\frac{1}{\eta^2}\left(m^2\pi^2-\frac{\kappa^2\beta^2}{\theta}+\frac{\theta}{\nu_1}\right), \tag{16a – d}$$

where

$$\lambda=\frac{a_1\mu^2+a_2\mu^2-a_3-a_5}{a_2\eta^2},\quad \alpha=\frac{a_1\mu^4-(a_3+a_4)\mu^2+a_6}{a_2\eta^4} \tag{17a,b}$$

and $a_i (i=1,2,\ldots,6)$ are given by Eqs. (A.2)–(A.7). Thus upon utilizing Eqs. (15a–c), α_1, α_2 and λ_3 can be determined. It is also shown that, to satisfy Eqs. (8a–c) after introducing Eqs. (12a–c), we have

$$C_1=\frac{\theta}{\alpha_1^2-\nu_1\alpha_3^2}=\frac{a_1\mu^2+a_2\eta^2\lambda_1^2-a_3}{\alpha_1^2},\quad C_2=\frac{\theta}{\alpha_2^2-\nu_1\alpha_3^2}=\frac{a_1\mu^2-a_2\eta^2\lambda_2^2-a_3}{\alpha_2^2}. \tag{18a,b}$$

3. Vibration and buckling criteria

In order to investigate the exact free vibration problem as well as obtaining the exact critical buckling load parameters of the rectangular plates for all the six combinations of boundary conditions shown in Fig. 2, we may assume:

$$\tilde{N}_1=\xi_1\tilde{N}_{cr},\quad \tilde{N}_2=\xi_2\tilde{N}_{cr}, \tag{19a,b}$$

where ξ_1 and ξ_2 are the scaling parameters and $\tilde{N}_{cr}$ is the dimensionless critical buckling load. Substituting Eqs. (A.2–A.7), given in Appendix A, into Eqs. (17a, b), we obtain

$$\lambda=\frac{\theta[(2\theta+\xi_1\tilde{N}_{cr}+\xi_2\tilde{N}_{cr})m^2\pi^2+\xi_2\tilde{N}_{cr}\theta]-\beta^2[\theta+(\theta+\xi_2\tilde{N}_{cr})\kappa^2\nu_1]}{(\theta+\tilde{K}_2+\xi_2\tilde{N}_{cr})\eta^2\theta}, \tag{20a}$$

$$\alpha=(\beta^4\kappa^2\nu_1-\beta^2\{\theta^2+[\theta+(\theta+\xi_2\tilde{N}_{cr})\kappa^2\nu_1]m^2\pi^2\}+[\xi_1\tilde{N}_{cr}(\theta+m^2\pi^2)]\theta m^2\pi^2+m^4\pi^4\theta^2)/((\theta+\xi_2\tilde{N}_{cr})\eta^4\theta), \tag{20b}$$

In view of Eqs. (15a–c) and Eq. (16c), Eqs. (18a, b) may also be written as

$$C_1=\frac{\theta^2}{\theta^2+\theta(\eta^2\lambda_1^2+m^2\pi^2)-\beta^2\kappa^2\nu_1}, \tag{21a}$$

$$C_2=\frac{\theta^2}{\theta^2-\theta(\eta^2\lambda_2^2-m^2\pi^2)-\beta^2\kappa^2\nu_1}, \tag{21b}$$

where λ_1 and λ_2 may be obtained from Eqs. (16a, b), respectively. Introducing Eqs. (14a–c) in Eqs. (12a–c) and substituting the results into the three appropriate boundary conditions along the edges $X_2=0$ and $X_2=1$ leads to a characteristic determinant of the six order for each m ($\mu=m\pi$, $m=1,2,\ldots$). Expanding the determinant and collecting terms yields a characteristic equation. The characteristic equations for all the six combinations of edge conditions are listed below:

Case 1. S-S-S-S

$$\sin\lambda_1\sinh\lambda_2\sinh\lambda_3=0. \tag{22}$$

Case 2. S-C-S-S

$$(C_1 - C_2)\mu^2 \tan\lambda_1 \tanh\lambda_2 - \eta^2\lambda_3(C_1\lambda_1 \tanh\lambda_2 - C_2\lambda_2 \tan\lambda_1)\tanh\lambda_3 = 0. \tag{23}$$

Case 3. S-C-S-C

$$\begin{aligned} &2(C_1 - C_2)\eta^2\mu^2\lambda_3[C_2\lambda_2(\cosh\lambda_2\cosh\lambda_3 - 1)\sin\lambda_1 - C_1\lambda_1(\cos\lambda_1\cosh\lambda_3 - 1)\sinh\lambda_2] \\ &\quad + [(C_1 - C_2)^2\mu^4 + (C_2^2\lambda_2^2 - C_1^2\lambda_1^2)\eta^4\lambda_3^2]\sin\lambda_1\sinh\lambda_2\sinh\lambda_3 \\ &\quad - 2C_1C_2\eta^4\lambda_3^2\lambda_1\lambda_2(\cos\lambda_1\cosh\lambda_2 - 1)\sinh\lambda_3 = 0. \end{aligned} \tag{24}$$

Case 4. S-S-S-F

$$C_2\lambda_1L_1L_2\tanh\lambda_2 + C_1\lambda_2L_3L_4\tan\lambda_1 - 2(C_1 - C_2)\eta^2\mu^2\lambda_1\lambda_2\lambda_3(1 - \nu)(1 + L_5)\tanh\lambda_3 = 0, \tag{25}$$

where

$$L_1 = (C_1 - 1 - L_5)\eta^2\lambda_3^2 - (C_1 + 1 + L_5)\mu^2, \quad L_2 = \eta^2\lambda_2^2 - \nu\mu^2, \tag{26a,b}$$

$$L_3 = (C_2 - 1 - L_5)\eta^2\lambda_3^2 - (C_2 + 1 + L_5)\mu^2, \quad L_4 = \eta^2\lambda_1^2 + \nu\mu^2, \tag{26c,d}$$

$$L_5 = \xi_2\tilde{N}_{cr}/\theta. \tag{26e}$$

Case 5. S-F-S-F

$$\begin{aligned} &4(C_1 - C_2)\eta^2\mu^2\lambda_1\lambda_2\lambda_3[C_1\lambda_2L_3L_4(\cos\lambda_1\cosh\lambda_3 - 1)\sinh\lambda_2 \\ &\quad - C_2\lambda_1L_1L_2(\cosh\lambda_2\cosh\lambda_3 - 1)\sin\lambda_1](1 - \nu) \\ &\quad + [4(C_1 - C_2)^2\eta^4\mu^4\lambda_1^2\lambda_2^2\lambda_3^2(1 - \nu)^2 + C_2^2\lambda_1^2L_1^2L_2^2 - C_1^2\lambda_2^2L_3^2L_4^2]\sin\lambda_1\sinh\lambda_2\sinh\lambda_3 \\ &\quad - 2C_1C_2\lambda_1\lambda_2L_1L_2L_3L_4(\cos\lambda_1\cosh\lambda_2 - 1)\sinh\lambda_3 = 0, \end{aligned} \tag{27}$$

Case 6. S-C-S-F

$$\begin{aligned} &\lambda_1\lambda_2\lambda_3\eta^2[C_2^2L_1L_2 - C_1^2L_3L_4 - 2(1 + L_5)(C_1 - C_2)^2\mu^4(1 - \nu)]\cos\lambda_1\cosh\lambda_2\cosh\lambda_3 \\ &\quad + (C_1 - C_2)C_2\lambda_1\mu^2\{[L_1L_2 - 2(1 + L_5)(1 - \nu)\lambda_2^2\lambda_3^2\eta^4]\sinh\lambda_2\sinh\lambda_3 \\ &\quad + \lambda_2\lambda_3\eta^2[L_1(1 - \nu) - 2L_2(1 + L_5)]\}\cos\lambda_1 \\ &\quad + (C_1 - C_2)C_1\lambda_2\mu^2\{[L_3L_4 - 2(1 + L_5)(1 - \nu)\lambda_1^2\lambda_3^2\eta^4]\sin\lambda_1\sinh\lambda_3 \\ &\quad - \lambda_1\lambda_3\eta^2[L_3(1 - \nu) + 2L_4(1 + L_5)]\}\cosh\lambda_2 \\ &\quad + C_1C_2\lambda_3\eta^2[(L_1L_2\lambda_1^2 + L_3L_4\lambda_2^2)\sin\lambda_1\sinh\lambda_2 + \lambda_1\lambda_2(L_1L_4 - L_2L_3)]\cosh\lambda_3 = 0. \end{aligned} \tag{28}$$

In Eqs. (22)–(28) λ_1 and λ_2 are related to λ and α given by Eqs. (20a, b) through relations expressed by Eqs. (16a, b).

For given values of ξ_1, ξ_2, θ, η and ν the characteristic equations are functions of β, m and $\tilde{N}_{cr}$. Depending on selection of ξ_1 and ξ_2, which may be either $(-1,0)$, $(0,-1)$ or $(-1,-1)$, the critical buckling load parameter $\tilde{N}_{cr}$ may be determined by setting $\beta = 0$ (i.e. zero natural frequency) in the corresponding characteristic equation of each individual cases. Upon testing the different integer values of m (usually $m = 1,2,3,\ldots$) the lowest value of solved equation is selected.

4. Comparison with known results

In order to validate the accuracy of the present method, a comparison has been carried out with previously published results by Leissa and Kang [15], Reddy and Phan [18], Kitipornchai et al. [30], Wang et al. [20], Shufrin and Eisenberger [35], Lam et al. [25], Liew et al. [19], Mizusawa [24] and Xiang [29] for both thin ($\delta = 0.001$) and moderately thick square rectangular plates for all the six considered boundary conditions. Plates are subjected to monoaxial in-plane compressive applied loads in the x_1 ($\xi_1 = -1$, $\xi_2 = 0$) and x_2 ($\xi_1 = 0$, $\xi_2 = -1$) directions and equal biaxial in-plane compressive applied loads ($\xi_1 = -1$, $\xi_2 = -1$).

Table 1
Comparison study of buckling load parameters, $\tilde{N}_{cr}/\pi^2 = N_{cr}a^2/\pi^2 D$, for square Mindlin plates having various boundary conditions and subjected to monoaxial in-plane compressive applied load in the X_1 direction ($\xi_1 = -1$, $\xi_2 = 0$)

Boundary conditions	Method	$\delta = h/a$			
		0.001	0.05	0.1	0.2
S-S-S-S	Mizusawa [24]	4	(3.928)	(3.729)	(3.119)
	Mizusawa [24]	4	3.944	3.784	3.256
	Present[a]	4	3.9437	3.7838	3.2558
	Shufrin and Eisenberger [35]	–	–	3.7865	3.2637
	Present[b]	4	3.9444	3.7864	3.2637
S-C-S-C	Mizusawa [24]	7.691	(7.228)	(6.178)	(4.056)
	Mizusawa [24]	7.691	7.299	6.370	4.320
	Present[a]	7.6911	7.2989	6.3698	4.3204
S-C-S-S	Mizusawa [24]	5.740	(5.574)	(5.140)	(3.876)
	Present[a]	5.7401	5.5977	5.2171	4.1364
S-C-S-F	Mizusawa [24]	1.653	(1.615)	(1.539)	(1.323)
	Mizusawa [24]	1.653	1.620	1.556	1.370
	Present[a]	1.6522	1.6197	1.5558	1.3701
S-S-S-F	Mizusawa [24]	1.402	(1.378)	(1.327)	(1.173)
	Present[a]	1.4014	1.3813	1.3707	1.2138
S-F-S-F	Mizusawa [24]	0.9523	(0.9412)	(0.9146)	(0.8274)
	Present[a]	0.95225	0.94314	0.92187	0.85011
	Shufrin and Eisenberger [35]	–	0.9433	0.9222	0.8512
	Present[b]	0.95225	0.94324	0.92222	0.85124

( ) Considering higher-order shear strain.
[a]Shear correction factor $\kappa^2 = \pi^2/12$.
[b]Shear correction factor $\kappa^2 = 5/6$.

The buckling load parameters $\tilde{N}_{cr}/\pi^2$ are listed in Tables 1 and 2 for $\delta = 0.001$, 0.05, 0.1 and 0.2 together with the available results by Mizusawa [24], obtained by using the spline strip method, and by Shufrin and Eisenberger [35], obtained by using the Levy method. It can be observed an excellent agreement between the present results and those given by Shufrin and Eisenberger [35]. Good agreement has also been achieved between the present results and those of Mizusawa [24]. Note that higher-order terms (in the transverse shear strain) have been considered in Mizusawa's [24] study. Those results are shown in parentheses in Tables 1 and 2 to distinguish them from the rest of results. Full agreement of the present results for S-S-S-S, S-C-S-F, S-S-S-F and S-F-S-F plates subjected to equal biaxial in-plane compressive loads ($\xi_1 = -1$, $\xi_2 = -1$) with the solutions of Liew et al. [21] and Xiang [29], obtained by using the *p*b-2 Rayleigh–Ritz method, is shown in Table 3 for both thin and moderately thick square rectangular plates.

5. Results and discussion

The critical buckling load parameters obtained from the exact characteristic equations presented in Section 3 have been expressed in dimensionless form $\tilde{N}_{cr} = N_{cr}a^2/D$, where the symbols are defined in Section 2. Numerical calculations have been performed for each of the six different boundary conditions shown in Fig. 2. In the numerical calculations, Poisson's ratio $\nu = 0.3$ and shear correction factor $\kappa^2 = 0.86667$ have been used. The results are given in Tables 4–9 for the thickness to length ratios $\delta = 0.001$, 0.001, 0.1, and 0.2 over a range of a aspect ratios $\eta = 0.4$, 0.5, 2/3, 1, 1.5, 2 and 2.5. In Tables 4–9, for each value of η and δ, the dimensionless critical buckling load parameters $\tilde{N}_{cr}$ are given for three in-plane loading cases, namely, monoaxial in-plane compressive load in the X_1-direction ($\xi_1 = -1$, $\xi_2 = 0$), monoaxial in-plane compressive

Table 2
Comparison study of buckling load parameters, $\tilde{N}_{cr}/\pi^2 = N_{cr}a^2/\pi^2 D$, for square Mindlin plates having various boundary conditions and subjected to monoaxial in-plane compressive applied load in the X_2 direction ($\xi_1 = 0$, $\xi_2 = -1$)

Boundary conditions	Method	δ			
		0.001	0.05	0.1	0.2
S-S-S-S	Mizusawa [24]	4	(3.928)	(3.729)	(3.119)
	Present[a]	4	3.9437	3.7838	3.2558
	Shufrin and Eisenberger [35]	–	–	3.7865	3.2637
	Present[b]	4	3.9444	3.78645	3.2637
S-C-S-C	Mizusawa [24]	6.743	(6.462)	(5.765)	(4.109)
	Present[a]	6.7431	6.5238	5.9487	4.4004
S-C-S-S	Mizusawa [24]	4.847	(4.717)	(4.372)	(3.418)
	Present[a]	4.8471	4.7454	4.4656	3.6115
S-C-S-F	Mizusawa [24]	2.392	(2.260)	(2.078)	(1.657)
	Liew et al.[19]	–	2.2667	2.1010	–
	Present[a]	2.3901	2.2667	2.1010	1.7200
S-S-S-F	Mizusawa [24]	2.366	(2.237)	(2.060)	(1.657)
	Liew et al.[19]	–	2.2442	2.0829	–
	Present[a]	2.3639	2.2442	2.0829	1.7105
S-F-S-F	Mizusawa [24]	2.043	(1.942)	(1.807)	(1.497)
	Liew et al.[19]	–	1.9456	1.8216	–
	Present[a]	2.0413	1.9457	1.8216	1.5333
	Shufrin and Eisenberger [35]	–	1.9469	1.8234	1.5372
	Present[b]	2.0413	1.9464	1.8234	1.5372

( ) Considering higher-order shear strain.
[a]Shear correction factor $\kappa^2 = \pi^2/12$.
[b]Shear correction factor $\kappa^2 = 5/6$.

Table 3
Comparison study of buckling load parameters, $\tilde{N}_{cr}/\pi^2 = N_{cr}a^2/\pi^2 D$, for square Mindlin plates having various boundary conditions and subjected to equal biaxial in-plane compressive applied loads ($\xi_1 = -1$, $\xi_2 = -1$)

Boundary conditions	Method	δ				
		0.001	0.005	0.05	0.1	0.2
S-S-S-S	Xiang [29]	2	–	1.9719	1.8920	1.7723
	Present[a]	2	1.9997	1.9718	1.8919	1.7722
S-C-S-F	Liew et al. [19]	–	1.1412	1.1119	1.0641	1.0049
	Present[b]	1.1431	1.1412	1.1119	1.0641	1.0049
S-S-S-F	Liew et al. [19]	–	1.0535	1.0323	0.99542	0.94760
	Present[b]	1.0548	1.0535	1.0322	0.99541	0.94758
S-F-S-F	Shufrin and Eisenberger [35]	–	–	0.9208	0.8977	0.8650
	Liew et al. [19]	–	0.93160	0.92071	0.89774	0.86505
	Present[b]	0.93209	0.93160	0.92071	0.89774	0.86504

[a]Shear correction factor $\kappa^2 = 0.823045$.
[b]Shear correction factor $\kappa^2 = 5/6$.

load in X_2-direction ($\xi_1 = 0$, $\xi_2 = -1$) and equal biaxial in-plane compressive loads ($\xi_1 = -1$, $\xi_2 = -1$). The results are presented with considerable accuracy simply because they were easily obtained to the accuracy given, and because they may be used as a benchmark.

Table 4
Buckling load parameters, $\tilde{N}_{cr} = N_{cr}a^2/D$, for S-S-S-S rectangular Mindlin plates ($\tilde{N}_1 = \xi_1\tilde{N}_{cr}, \tilde{N}_2 = \xi_2\tilde{N}_{cr}$).

(ξ_1, ξ_2)	δ	$\eta = 0.4$		$\eta = 0.5$		$\eta = 2/3$		$\eta = 1$		$\eta = 1.5$		$\eta = 2$		$\eta = 2.5$	
		$\tilde{N}_{cr}$	m	$\tilde{N}_{cr}$	m	$\tilde{N}_{cr}$	m	$\tilde{N}_{cr}$	m	$\tilde{N}_{cr}$	m	$\tilde{N}_{cr}$	m	$\tilde{N}_{cr}$	m
(−1,0)	0.001	13.280498	1	15.421205	1	20.592057	1	39.478204	1	96.381222	1	157.910245	1	255.022775	3
	0.01	13.276364	1	15.416032	1	20.584076	1	39.457021	1	96.219798	1	157.571876	1	253.983122	3
	0.1	12.875571	1	14.915722	1	19.816043	1	37.447690	1	82.416286	1	129.765726	1	180.427919	6
	0.2	11.796432	1	13.580179	1	17.803107	1	32.441432	1	57.444097	1	76.902078	1	87.667294	6
(0,−1)	0.001	40.805061	1	39.478203	1	42.836502	1	39.478203	1	46.331901	1	61.684191	1	83.001741	1
	0.01	40.778353	1	39.457021	1	42.804585	1	39.457021	1	46.291517	1	61.601514	1	82.840527	1
	0.1	38.273227	1	37.447690	1	39.836454	1	37.447690	1	42.580103	1	54.320716	1	69.367296	1
	0.2	32.266500	1	32.441432	1	32.919274	1	32.441432	1	34.257183	1	39.995897	1	46.466346	1
(−1,−1)	0.001	11.448705	1	12.336964	1	14.256039	1	19.739102	1	32.075932	1	49.347353	1	71.553225	1
	0.01	11.445141	1	12.332826	1	14.250514	1	19.728510	1	32.047973	1	49.281211	1	71.414247	1
	0.1	11.099630	1	11.932578	1	13.718799	1	18.723845	1	29.478533	1	43.456572	1	59.799393	1
	0.2	10.169338	1	10.864143	1	12.325227	1	16.220716	1	23.716511	1	31.996718	1	40.057195	1

Table 5
Buckling load parameters, $\tilde{N}_{cr} = N_{cr}a^2/D$, for S-C-S-S rectangular Mindlin plates ($\tilde{N}_1 = \xi_1\tilde{N}_{cr}, \tilde{N}_2 = \xi_2\tilde{N}_{cr}$)

(ξ_1, ξ_2)	δ	$\eta = 0.4$		$\eta = 0.5$		$\eta = 2/3$		$\eta = 1$		$\eta = 1.5$		$\eta = 2$		$\eta = 2.5$	
		$\tilde{N}_{cr}$	m	$\tilde{N}_{cr}$	m	$\tilde{N}_{cr}$	m	$\tilde{N}_{cr}$	m	$\tilde{N}_{cr}$	m	$\tilde{N}_{cr}$	m	$\tilde{N}_{cr}$	m
(−1,0)	0.001	13.989148	1	16.909363	1	24.588768	1	56.653026	1	120.605362	1	221.289125	1	334.506381	3
	0.01	13.984260	1	16.902466	1	24.575333	1	56.598315	1	120.300623	1	220.209713	1	332.320553	3
	0.1	13.515706	1	16.247894	1	23.325285	1	51.727083	1	96.958820	1	151.127293	1	202.956572	4
	0.2	12.284667	1	14.573567	1	20.299130	1	41.394657	1	62.550161	1	78.916068	1	88.028497	6
(0,−1)	0.001	41.121939	1	41.814166	1	44.381101	1	47.839054	1	68.730339	1	102.507741	1	147.211382	1
	0.01	41.098866	1	41.788087	1	44.353494	1	47.800457	1	68.623785	1	102.240646	1	146.628809	1
	0.1	38.872664	1	39.327498	1	41.680705	1	44.250502	1	59.522778	1	81.347872	1	105.465834	1
	0.2	33.007680	1	33.270595	1	34.672932	1	36.117964	1	42.767223	1	50.785399	1	57.741531	1
(−1,−1)	0.001	11.906476	1	13.237267	1	16.365561	1	26.279529	1	50.348550	1	85.078680	1	130.173604	1
	0.01	11.902468	1	13.232180	1	16.357440	1	26.257608	1	50.268168	1	84.852919	1	129.652278	1
	0.1	11.516459	1	12.745925	1	15.592868	1	24.266084	1	43.440418	1	67.249248	1	92.895600	1
	0.2	10.492953	1	11.483084	1	13.692782	1	19.834657	1	31.021458	1	41.693257	1	50.526135	1

5.1. Analysis of linear buckling mode shapes

For each dimensionless critical buckling load parameter, the corresponding mode shape is described by the number of half-waves in the X_1- and X_2-directions, respectively. For example, an S-C-S-S plate subjected to monoaxial in-plane compressive load in the X_1-direction has five half-waves ($m = 5$) in the X_1-direction and one ($n = 1$) in the X_2-direction in its critical buckling mode shape for $\eta = 2.5$ and $\delta = 0.18$. The critical buckling mode shapes for all the six considered boundary conditions subjected to monoaxial in-plane compressive load in the X_1-direction ($\xi_1 = -1$, $\xi_2 = 0$) have a single half-wave in the X_2-direction. For plates subjected to the monoaxial in-plane load in the X_2-direction, the critical buckling mode shapes for all the six considered plates subjected to monoaxial in-plane compressive load in the X_2-direction ($\xi_1 = 0$, $\xi_2 = -1$) have a single half-wave in the X_1-direction ($m = 1$); that is, no nodal lines along the unloaded edges exist. Similar to the loading configuration as described by ($\xi_1 = -1$, $\xi_2 = 0$), the critical buckling mode shapes for all six considered plates within the range of η and δ given in Tables 4–9, have a single half-wave in the X_1-direction ($n = 1$), when the loading configuration changes to ($\xi_1 = -1$, $\xi_2 = -1$). However, there is possibility of

Table 6
Buckling load parameters, $\tilde{N}_{cr} = N_{cr}a^2/D$, for S-C-S-C rectangular Mindlin plates ($\tilde{N}_1 = \xi_1\tilde{N}_{cr}, \tilde{N}_2 = \xi_2\tilde{N}_{cr}$)

(ξ_1, ξ_2)	δ	$\eta = 0.4$		$\eta = 0.5$		$\eta = 2/3$		$\eta = 1$		$\eta = 1.5$		$\eta = 2$		$\eta = 2.5$	
		$\tilde{N}_{cr}$	m	$\tilde{N}_{cr}$	m	$\tilde{N}_{cr}$	m	$\tilde{N}_{cr}$	m	$\tilde{N}_{cr}$	m	$\tilde{N}_{cr}$	m	$\tilde{N}_{cr}$	m
(−1,0)	0.001	14.919490	1	18.977382	1	30.580624	1	75.908333	1	158.014518	1	275.207980	1	431.679400	4
	0.01	14.913439	1	18.967541	1	30.556443	1	75.751492	1	157.410593	1	273.274597	1	426.850398	4
	0.1	14.342008	1	18.055467	1	28.388438	1	63.404106	1	116.406548	1	168.416063	1	217.402563	4
	0.2	12.890890	1	15.851026	1	23.616847	1	43.567623	1	65.506456	1	80.032333	1	88.307519	7
(0,−1)	0.001	44.633691	1	47.839054	1	53.045569	1	66.551761	1	111.846806	1	179.494196	1	267.644593	1
	0.01	44.605700	1	47.800462	1	53.006792	1	66.467258	1	111.552969	1	178.685138	1	265.797003	1
	0.1	41.951350	1	44.250506	1	49.333458	1	59.064064	1	88.632854	1	123.678040	1	157.959031	1
	0.2	35.234905	1	36.117969	1	40.017850	1	44.221938	1	55.045273	1	64.520463	1	71.392578	1
(−1,−1)	0.001	12.566475	1	14.617368	1	19.834763	1	37.799103	1	83.662918	1	150.984923	1	231.834547	2
	0.01	12.561725	1	14.610535	1	19.821224	1	37.749567	1	83.439474	1	150.299431	1	230.060685	2
	0.1	12.109220	1	13.969074	1	18.583660	1	33.470909	1	66.104129	1	100.715609	1	132.908965	2
	0.2	10.938568	1	12.373489	1	15.733275	1	25.178902	1	41.013668	1	52.357277	1	60.508358	2

Table 7
Buckling load parameters, $\tilde{N}_{cr} = N_{cr}a^2/D$, for S-S-S-F rectangular Mindlin plates ($\tilde{N}_1 = \xi_1\tilde{N}_{cr}, \tilde{N}_2 = \xi_2\tilde{N}_{cr}$)

(ξ_1, ξ_2)	δ	$\eta = 0.4$		$\eta = 0.5$		$\eta = 2/3$		$\eta = 1$		$\eta = 1.5$		$\eta = 2$		$\eta = 2.5$	
		$\tilde{N}_{cr}$	m	$\tilde{N}_{cr}$	m	$\tilde{N}_{cr}$	m	$\tilde{N}_{cr}$	m	$\tilde{N}_{cr}$	m	$\tilde{N}_{cr}$	m	$\tilde{N}_{cr}$	m
(−1,0)	0.001	10.388390	1	10.746877	1	11.536996	1	13.831383	1	19.042797	1	26.366058	1	35.793556	1
	0.01	10.382133	1	10.739327	1	11.526539	1	13.811088	1	18.992415	1	26.258793	1	35.593483	1
	0.1	10.075046	1	10.408425	1	11.142211	1	13.257101	1	17.977429	1	24.457914	1	32.598809	1
	0.2	9.299893	1	9.590606	1	10.229108	1	12.054586	1	16.058631	1	21.430636	1	28.011069	1
(0,−1)	0.001	22.781855	1	22.782251	1	22.730519	1	23.331097	1	22.879899	1	20.147421	1	18.152513	1
	0.01	22.614851	1	22.615032	1	22.565404	1	23.154752	1	22.709213	1	20.001311	1	18.008016	1
	0.1	20.247457	1	20.246817	1	20.217433	1	20.646926	1	20.353316	1	18.047075	1	16.149397	1
	0.2	16.843522	1	16.843153	1	16.829688	1	17.074388	1	16.973422	1	15.284579	1	13.632384	1
(−1,−1)	0.001	9.716299	1	9.793934	1	9.966750	1	10.410867	1	11.125024	1	11.736470	1	12.204967	1
	0.01	9.702060	1	9.777844	1	9.946938	1	10.381657	1	11.078379	1	11.670336	1	12.118570	1
	0.1	9.329653	1	9.384918	1	9.511919	1	9.840696	1	10.347413	1	10.735373	1	10.978016	1
	0.2	8.523821	1	8.557420	1	8.638288	1	8.850842	1	9.158155	1	9.344447	1	9.393642	1

existence of higher order n. Inspecting the critical buckling mode shapes for the some values of $\eta > 2.5$, confirms the existence of the mode shapes which may be described by ($m = 1, n = 2$). Inspection of Tables 4–9 also indicates that, within the range of η and δ given in these tables, the variety of the critical buckling mode shapes for all the six considered plates may be expressed by (1,1), (2,1), (3,1), (4,1), (5,1), (6,1) and (7,1) modes for plates subjected to monoaxial load in the X_1-direction ($\xi_1 = -1$, $\xi_2 = 0$). Similarly, the critical mode shapes are limited to (1,1), (1,2) and (1,3) modes for plates subjected to monoaxial load in the X_2-direction ($\xi_1 = 0$, $\xi_2 = -1$), and to (1,1) and (2,1) modes for plates subjected to equal biaxial loads ($\xi_1 = -1$, $\xi_2 = -1$). The typical critical buckling mode shapes for plates with thickness ratio $\delta = 0.2$ and aspect ratios $\eta = 2.5$ and 0.4 are given by contour plots in Figs. 3 and 4. These figures show the shape of the buckled plate in each mode, for all the six different boundary conditions and all the three types of in-plane loading cases considered. The mathematical expression of mode shapes are given in Appendix C. For all the six cases the wave forms are sine functions in the X_1-direction. The wave forms in the X_2-direction are sine function exactly for the S-S-S-S case only, whereas for the other cases the forms are only approximately sinusoidal. As a consequence, it can be observed in Figs. 3 and 4 that the nodal lines (for transverse displacement) lying in the X_2-direction (five for a

Table 8
Buckling load parameters, $\tilde{N}_{cr} = N_{cr}a^2/D$, for S-F-S-F rectangular Mindlin plates ($\tilde{N}_1 = \xi_1\tilde{N}_{cr}, \tilde{N}_2 = \xi_2\tilde{N}_{cr}$)

(ξ_1, ξ_2)	δ	$\eta = 0.4$		$\eta = 0.5$		$\eta = 2/3$		$\eta = 1$		$\eta = 1.5$		$\eta = 2$		$\eta = 2.5$	
		$\tilde{N}_{cr}$	m	$\tilde{N}_{cr}$	m	$\tilde{N}_{cr}$	m	$\tilde{N}_{cr}$	m	$\tilde{N}_{cr}$	m	$\tilde{N}_{cr}$	m	$\tilde{N}_{cr}$	m
(−1,0)	0.001	9.651388	1	9.604314	1	9.529572	1	9.398358	1	9.255947	1	9.167625	1	9.113162	1
	0.01	9.646287	1	9.598768	1	9.523357	1	9.391159	1	9.248205	1	9.160045	1	9.106003	1
	0.1	9.375177	1	9.325573	1	9.247239	1	9.112050	1	8.971891	1	8.891002	1	8.844839	1
	0.2	8.679801	1	8.632796	1	8.558944	1	8.434126	1	8.312382	1	8.248819	1	8.216368	1
(0,−1)	0.001	22.722608	1	22.295281	1	22.252165	1	20.147421	1	16.914476	1	15.594572	1	14.956221	1
	0.01	22.555180	1	22.135788	1	22.091907	1	20.001311	1	16.761460	1	15.413724	1	14.742174	1
	0.1	20.199385	1	19.883230	1	19.807348	1	18.047074	1	14.863227	1	13.292184	1	12.325797	1
	0.2	16.817774	1	16.624882	1	16.521587	1	15.284578	1	12.399596	1	10.724113	1	9.550652	1
(−1,−1)	0.001	9.456449	1	9.399642	1	9.317343	1	9.199447	1	9.104095	1	9.057540	1	9.032521	1
	0.01	9.445386	1	9.388217	1	9.305541	1	9.187754	1	9.093588	1	9.048318	1	9.024358	1
	0.1	9.117073	1	9.060047	1	8.979102	1	8.871143	1	8.797076	1	8.769022	1	8.757980	1
	0.2	8.373065	1	8.323660	1	8.255286	1	8.173842	1	8.134317	1	8.129924	1	8.134328	1

Table 9
Buckling load parameters, $\tilde{N}_{cr} = N_{cr}a^2/D$, for S-C-S-F rectangular Mindlin plates ($\tilde{N}_1 = \xi_1\tilde{N}_{cr}, \tilde{N}_2 = \xi_2\tilde{N}_{cr}$)

(ξ_1, ξ_2)	δ	$\eta = 0.4$		$\eta = 0.5$		$\eta = 2/3$		$\eta = 1$		$\eta = 1.5$		$\eta = 2$		$\eta = 2.5$	
		$\tilde{N}_{cr}$	m	$\tilde{N}_{cr}$	m	$\tilde{N}_{cr}$	m	$\tilde{N}_{cr}$	m	$\tilde{N}_{cr}$	m	$\tilde{N}_{cr}$	m	$\tilde{N}_{cr}$	m
(−1,0)	0.001	10.517837	1	11.012034	1	12.203649	1	16.306648	1	28.663682	1	52.718216	1	85.401986	2
	0.01	10.511051	1	11.003412	1	12.190336	1	16.274002	1	28.558937	1	52.457263	1	84.829241	2
	0.1	10.189581	1	10.642566	1	11.726966	1	15.394207	1	26.121935	1	46.387846	1	68.346156	2
	0.2	9.387772	1	9.769217	1	10.669775	1	13.627190	1	21.886378	1	36.692284	1	46.501252	2
(0,−1)	0.001	22.783449	1	22.785246	1	22.907573	1	23.590060	1	23.847247	1	25.897575	1	30.158359	1
	0.01	22.616341	1	22.618063	1	22.738384	1	23.407796	1	23.662029	1	25.692630	1	29.919152	1
	0.1	20.248073	1	20.249192	1	20.332618	1	20.827396	1	21.072611	1	22.727222	1	26.195608	1
	0.2	16.843679	1	16.844266	1	16.884265	1	17.171725	1	17.423632	1	18.598532	1	20.997708	1
(−1,−1)	0.001	9.759345	1	9.869577	1	10.211032	1	11.282178	1	14.010953	1	18.093580	1	23.493915	1
	0.01	9.744070	1	9.866929	1	10.186771	1	11.239951	1	13.931286	1	17.969432	1	23.321253	1
	0.1	9.359405	1	9.452941	1	9.694772	1	10.523468	1	12.710612	1	16.061858	1	20.517889	1
	0.2	8.540609	1	8.598204	1	8.754655	1	9.319684	1	10.888515	1	13.343285	1	16.561900	1

(6,1) mode) are evenly spaced. On the other hand those lying in the X_2-direction (two for a (1,3) mode), except for the S-S-S-S case, are not evenly spaced.

The critical buckling mode shapes given in Figs. 3 and 4, where the double geometric symmetry exist (e.g., S-S-S-S , S-C-S-C and S-F-S-F) may be classified as X_2-symmetric or X_2-antisymmetric modes depend on whether or not having an axis of symmetry with respect to the X_2-coordinate. According to this classification (1,1), (1,2), (1,3) and (7,1) modes are X_2-symmetric modes, where as (2,1) mode is an X_2-antisymmetric mode.

The close examination of the contour plots also suggest that the modes can be classified into four distinct symmetry classes: namely, double-symmetry modes (SS), symmetry–antisymmetry modes (SA), antisymmetry–symmetry modes (AS) and double-antisymmetry modes (AA), about the midplanes parallel to the X_1–X_3 and X_2–X_3 planes. According to these symmetry classes ((1,1), (1,3), (7,1)), ((2,1), (6,1)) and (1,2) modes in Figs. 3 and 4 may be given as an examples of SS, SA, and AS modes, respectively. On the other hand ((1,1), (1,2), (1,3)) and ((2,1), (6,1)) modes in Figs. 3 and 4 may be given as an example of AS and AA modes, respectively. Note that where there is no geometric symmetry along the edges parallel to the X_1-axis, the contours are not symmetric about the midplane parallel to the X_1–X_3 plane.

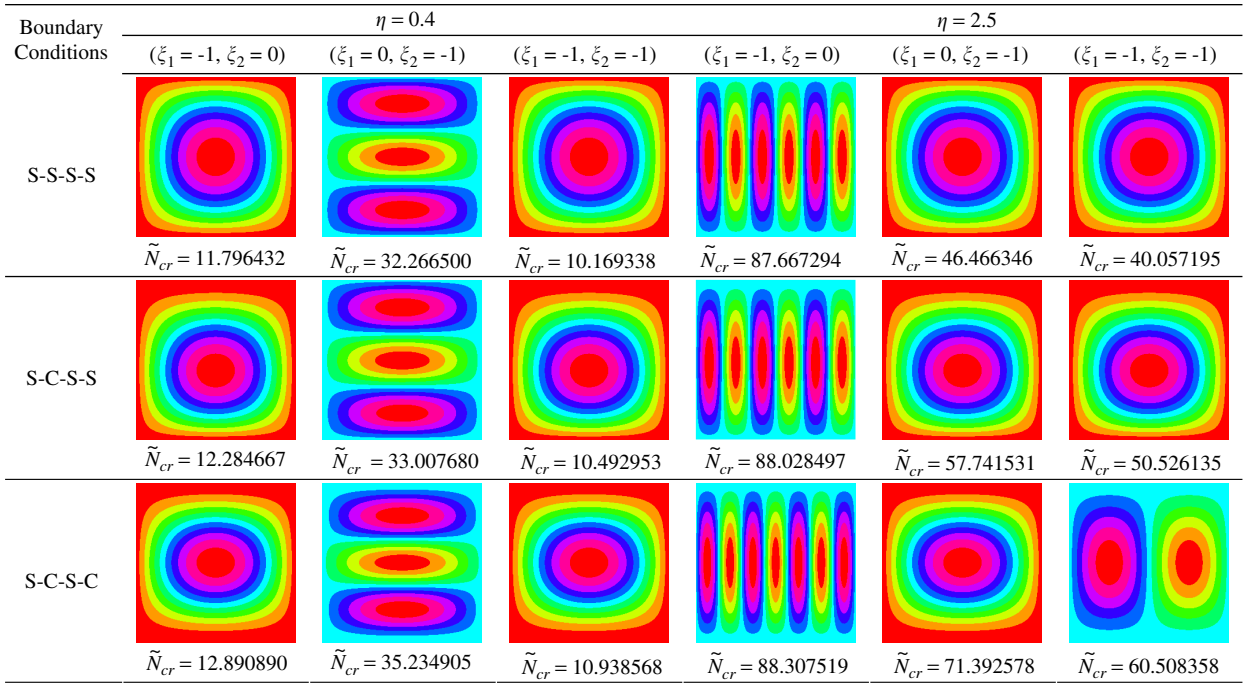

Fig. 3. Buckling mode shapes of rectangular Mindlin plates for S-S-S-S, S-C-S-S and S-C-S-C boundary conditions.

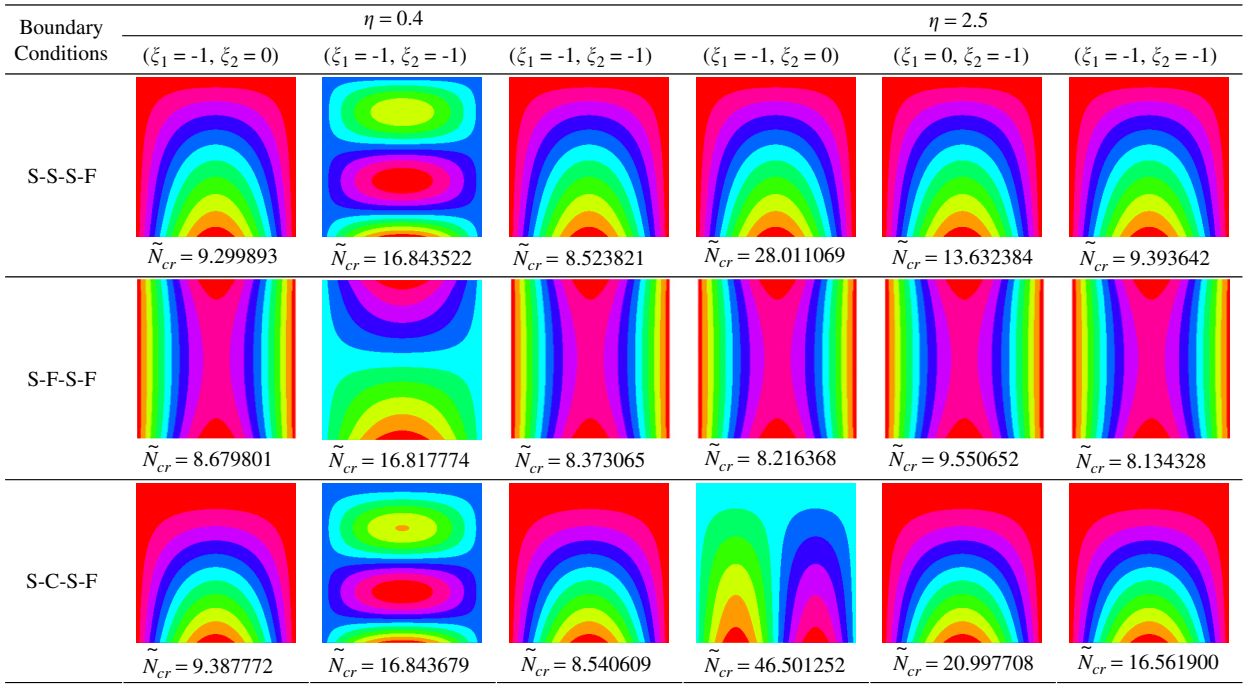

Fig. 4. Buckling mode shapes of rectangular Mindlin plates for S-S-S-F, S-F-S-F and S-C-S-F boundary conditions.

5.2. *Effect of aspect ratio on the critical buckling load*

In order to study the effect of the aspect ratio on the buckling of plates, attention is focused on Tables 4–9. It is observed that for the loading case ($\xi_1 = -1,\ \xi_2 = 0$), the dimensionless critical buckling loads $\tilde{N}_{cr}$,

except for S-F-S-F plates, increase with the plate aspect ratio η keeping the thickness ratio δ constant. This observation indicates that, between two plates having identical length a, thickness h and boundary conditions, the one which has shorter width b reaches to instability under greater monoaxial in-plane compressive applied load in the X_1-direction. Unlike the rest of plates, the S-F-S-F plates behave differently. For these plates the dimensionless critical buckling loads decrease with increasing plate aspect ratio η. Consider now Fig. 5 which presents variations of $\tilde{N}_{cr}/\eta^2 = N_{cr}b^2/D$ versus η for all the six boundary conditions for the loading case ($\xi_1 = -1$, $\xi_2 = 0$). Results show the variation of the critical buckling load (not the dimensionless one) in plates having an identical width b, thickness h and boundary conditions as a function of the length of the plates in t he direction of the in-plane compressive applied load. One may also note that, for plates with S-S-S-F and S-F-S-F boundary conditions, the number of half-waves along the X_1-direction (m) remain unchanged for the critical mode by increasing η.

From Tables 4–9 one may study the variation of $\tilde{N}_{cr}/\eta^2 = N_{cr}b^2/D$ versus η for plates subjected to monoaxial in-plane compressive load in the X_2-direction ($\xi_1 = 0$, $\xi_2 = -1$). For all the six considered plates, the values of $\tilde{N}_{cr}/\eta^2 = N_{cr}b^2/D$ decrease with increasingη. Note that for all the six considered plates subjected to monoaxial in-plane compressive load in the X_2-direction, there are no free edges along the direction parallel to the applied in-plane load. Regardless of direction of the applied monoaxial in-plane load, between two

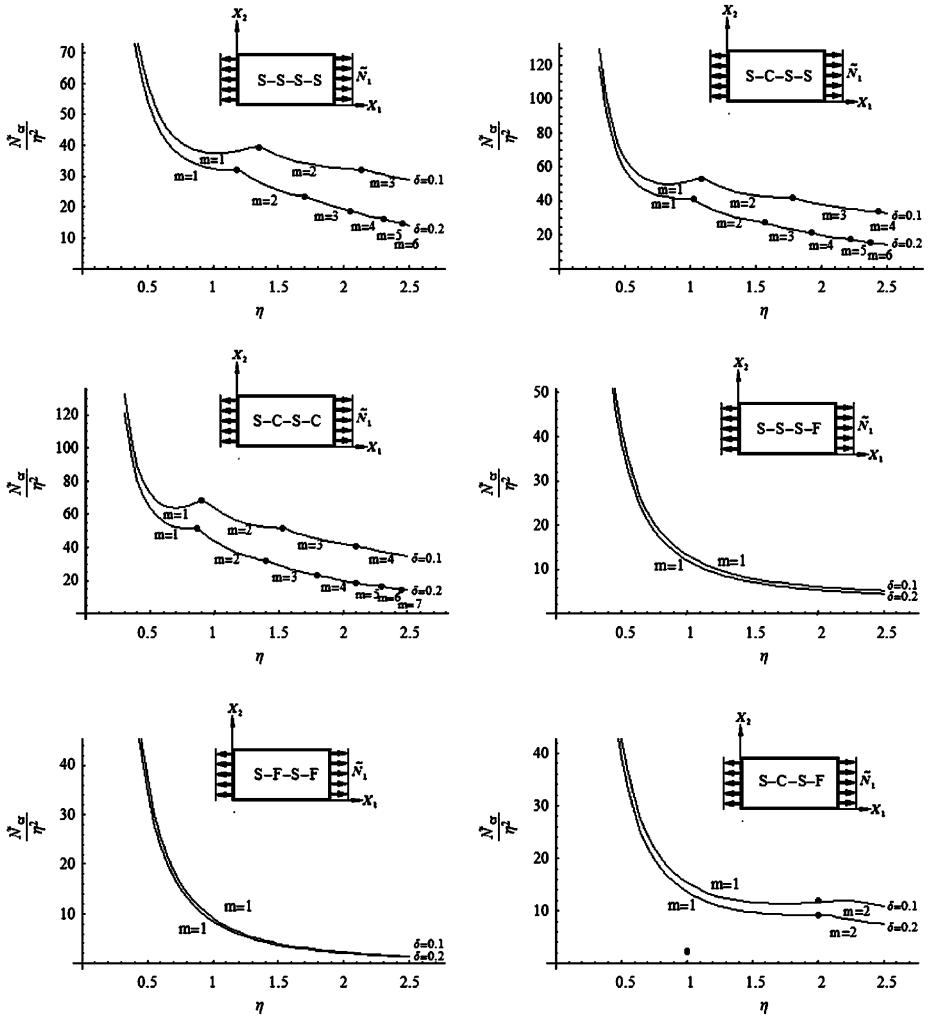

Fig. 5. Variations of buckling load parameters $\tilde{N}_{cr}/\eta^2 = N_{cr}b^2/D$ versus η, for rectangular Mindlin plates having various boundary conditions and subjected to monoaxial in-plane compressive applied loads ($\xi_1 = -1$, $\xi_2 = 0$).

plates having identical thickness h and boundary conditions, the one which has smaller side along the applied load reaches instability under larger load, provided that the dimensions of the other two edges are the same. This is true except for the S-F-S-F plates subjected to monoaxial in-planes compressive load in the X_1-direction.

From the results presented in Tables 4–9, it is observed that for the loading case described as ($\xi_1 = 0$, $\xi_2 = -1$), the dimensionless critical buckling load $\tilde{N}_{cr}$, for plate having S-C-S-S, S-C-S-C and S-C-S-F boundary conditions, increases with η if the thickness ratio δ is kept constant. A typical variation of $\tilde{N}_{cr}$ versus η for all the six considered plates with thickness ratio $\delta = 0.1$ is given in Fig. 6. The range of η with the same number of half-waves in the X_2-direction (n) is indicated by dots in the figure. Inspection of curves given in Fig. 6, gives an idea of how the critical buckling loads vary in plates having an identical length a, thickness h and boundary conditions versus the width b.

Consideration may now be focused on plates subjected to equal biaxial in-plane compressive loads ($\xi_1 = -1$, $\xi_2 = -1$). From the results presented in Tables 4–9, it is observed that for this loading case, the dimensionless critical buckling load $\tilde{N}_{cr}$, expect for the S-F-S-F plates, increase with the aspect ratio η if the thickness ratio δ is kept constant. For plates with S-F-S-F boundary conditions, results presented in Table 8 indicated that the value of $\tilde{N}_{cr}$ initially decrease with increasingη. The change of this initially decreasing trend to the increasing one, within the range of η and δ covered in Table 5, may be observed for $\delta = 0.2$ for values of η of 2 and 2.5. In particular, variations of $\tilde{N}_{cr}$ versus η are shown in Fig. 7 for $\delta = 0.1$, 0.14 and 0.2. The position at which the number of half-waves in the X_2-direction changes from $n = 1$ to 2 are also specified with

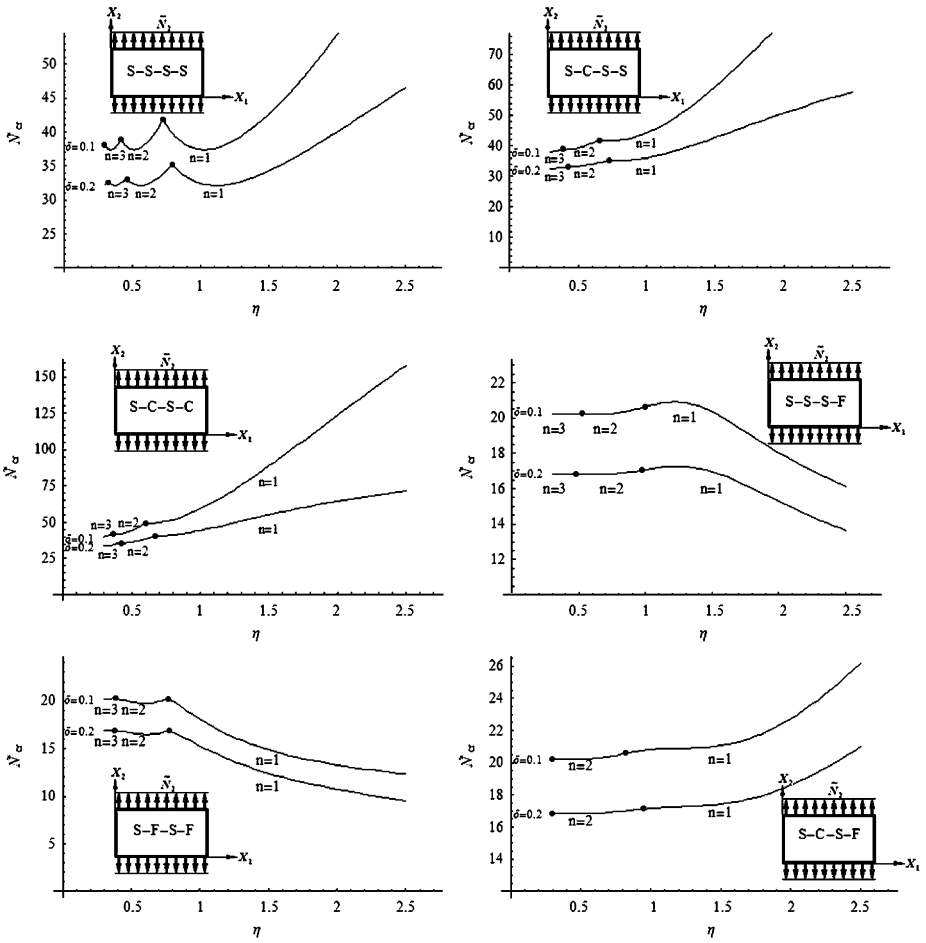

Fig. 6. Variations of buckling load parameters $\tilde{N}_{cr}/\eta^2 = N_{cr}a^2/D$ versus η, for rectangular Mindlin plates having various boundary conditions and subjected to monoaxial in-plane compressive applied loads ($\xi_1 = 0$, $\xi_2 = -1$).

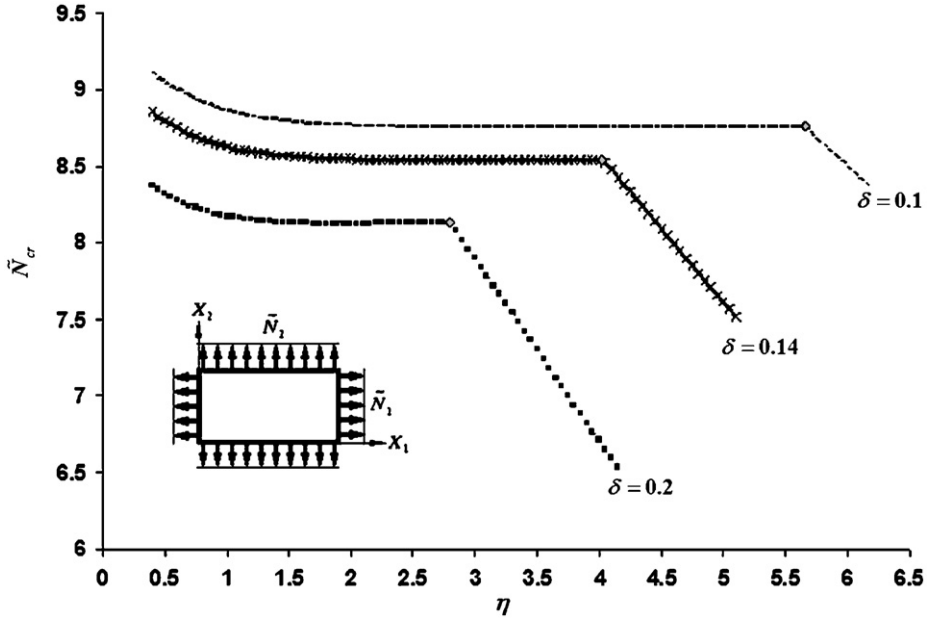

Fig. 7. Variations of buckling load parameters $\tilde{N}_{cr}/\eta^2 = N_{cr}a^2/D$ versus η, for rectangular Mindlin plates with S-F-S-F boundary condition and subjected to equal biaxial in-plane compressive applied loads ($\xi_1 = -1$, $\xi_2 = -1$).

the symbol ●. It is seen that by increasing δ the critical buckling mode shapes are shifted from (1,1) to (1,2) for smaller values of η.

Fig. 8 presents the typical variations of $\tilde{N}_{cr}/\eta^2 = N_{cr}b^2/D$ versus η for all the six considered plates subjected to equal biaxial in-plane compressive applied loads. From the curves given in Fig. 8, it is seen that, for all the six cases, the values of $\tilde{N}_{cr}/\eta^2 = N_{cr}b^2/D$ decrease with η.

5.3. Effect of thickness ratio on the critical buckling load

The influence of the thickness ratio δ on the nondimensional critical buckling loads for plates with specific boundary conditions can also be examined by keeping the aspect ratio constant while varying the thickness ratio. From the results presented in Tables 4–9 it can be easily observed that, as the thickness ratio δ increases from 0.001 to 0.2, the nondimensional critical buckling load decreases. Such behavior is due to the influence of the transverse shear deformation in the plates. Moreover, it can be observed that shear deformation not only reduces the values of $\tilde{N}_{cr}$, but also cause changes in the buckling shapes. As an example, for S-S-S-S plates with aspect ratio $\eta = 2.5$ subject to monoaxial in-plane compressive load in the X_1-direction, the number of half-waves (m) varies from 3 to 6 as the values of δ increases from 0.001 to 0.2.

5.4. Effect of boundary conditions on the critical buckling load

To study the effect of boundary conditions on the dimensionless critical buckling loads, the values of $\tilde{N}_{cr}$ listed in a specific row and column of Tables 4–9 may be selected from each table for each loading case and arranged in terms of boundary conditions as shown in Table 10. From the results presented in this table, it is observed that the lowest dimensionless critical buckling loads correspond to plates with less constraints. As the number of supported edges increases, the values of $\tilde{N}_{cr}$ also increase. Among all the six boundary conditions considered in Table 10, it can be seen that the lowest and highest values of $\tilde{N}_{cr}$ correspond to S-F-S-F and S-C-S-C cases, respectively. Thus, constraints at the edges increase the flexural rigidity of the plate, resulting in a higher critical buckling load.

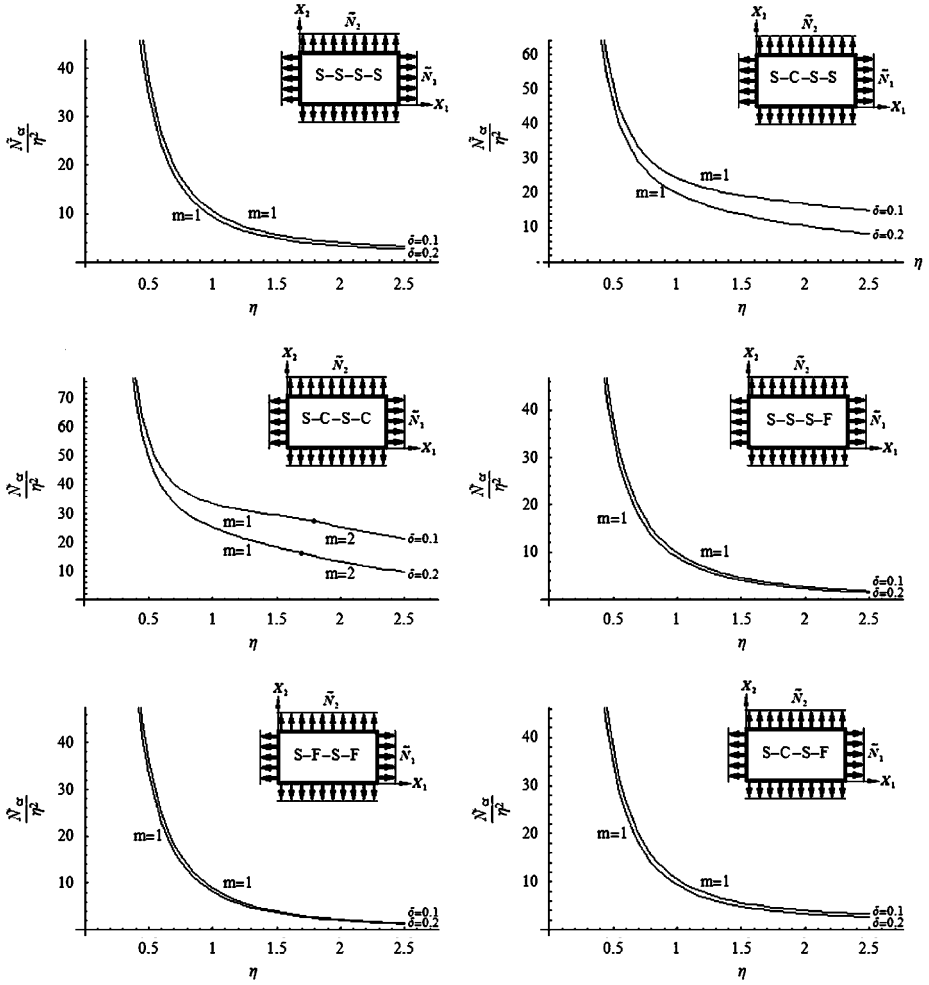

Fig. 8. Variations of buckling load parameters $\tilde{N}_{cr}/\eta^2 = N_{cr}b^2/D$ versus η, for rectangular Mindlin plates having various boundary conditions and subjected to equal biaxial in-plane compressive applied loads ($\xi_1 = -1$, $\xi_2 = -1$).

In order to study the effect of the shear correction factor on the dimensionless critical buckling loads, attention is placed again to Table 10. From the results presented in this table, it is observed that, for all of the loading cases, the dimensionless critical buckling load $\tilde{N}_{cr}$ increase with the shear correction factor.

5.5. Complementary results

In order to satisfy Eq. (22) (case of S-S-S-S boundary conditions), it is necessary that $\lambda_1 = n\pi$ with integer values of n. Thus for this case (and only this case), the dimensionless critical buckling load can be determined explicitly:

$$\tilde{N}_{cr} = -\frac{\theta\pi^2(m^2 + n^2\eta^2)^2}{(m^2\pi^2 + n^2\pi^2\eta^2 + \theta)(m^2\xi_1 + n^2\eta^2\xi_2)}. \tag{29}$$

For plates subjected to monoaxial in-plane compressive load in the X_1-direction ($\xi_1 = -1$, $\xi_2 = 0$) we obtain:

$$N_{x1} = -\frac{\theta\pi^2(m^2 + n^2\eta^2)^2}{(m^2\pi^2 + n^2\pi^2\eta^2 + \theta)m^2}, \tag{30}$$

Table 10
Effects of shear deformation on buckling load parameters, $\tilde{N}_{cr} = N_{cr}a^2/D$, for different boundary conditions of rectangular Mindlin plates with $\eta = 1.5$, $\delta = 0.2$

Boundary conditions	Loading cases		
	$(\xi_1 = -1, \xi_2 = 0)$	$(\xi_1 = 0, \xi_2 = -1)$	$(\xi_1 = -1, \xi_2 = -1)$
S-F-S-F	(8.42030)[a] (11)	(12.74146)[a] (12)	(8.24146)[a] (11)
	(8.31238)[b] (11)	(12.39959)[b] (12)	(8.13431)[b] (11)
	(8.28064)[c] (11)	(12.30198)[c] (12)	(8.10287)[c] (11)
	(8.26979)[d] (11)	(12.26894)[d] (12)	(8.09213)[d] (11)
S-S-S-F	(16.35437)[a] (11)	(17.45472)[a] (11)	(9.33528)[a] (11)
	(16.05363)[b] (11)	(16.97342)[b] (11)	(9.15815)[b] (11)
	(15.97262)[c] (11)	(16.83549)[c] (11)	(9.10693)[c] (11)
	(15.94336)[d] (11)	(16.78876)[d] (11)	(9.08953)[d] (11)
S-C-S-F	(22.49508)[a] (11)	(17.93638)[a] (11)	(11.14802)[a] (11)
	(21.88637)[b] (11)	(17.42363)[b] (11)	(10.88851)[b] (11)
	(21.71217)[c] (11)	(17.27709)[c] (11)	(10.81416)[c] (11)
	(21.65318)[d] (11)	(17.22749)[d] (11)	(10.78897)[d] (11)
S-S-S-S	(60.71451)[a] (21)	(35.49042)[a] (11)	(24.57029)[a] (11)
	(57.44409)[b] (21)	(34.25718)[b] (11)	(23.71651)[b] (11)
	(56.53047)[c] (21)	(33.90370)[c] (11)	(23.47179)[c] (11)
	(56.22333)[d] (21)	(33.78397)[d] (11)	(23.38890)[d] (11)
S-C-S-S	(66.66637)[a] (21)	(44.99570)[a] (11)	(32.66068)[a] (11)
	(62.55016)[b] (21)	(42.76722)[b] (11)	(31.02145)[b] (11)
	(61.41673)[c] (21)	(42.14227)[c] (11)	(30.56256)[c] (11)
	(61.03725)[d] (21)	(41.93193)[d] (11)	(30.40819)[d] (11)
S-C-S-C	(71.10860)[a] (31)	(59.00146)[a] (11)	(43.94142)[a] (11)
	(65.50645)[b] (31)	(55.04527)[b] (11)	(41.01366)[b] (11)
	(63.99777)[c] (31)	(53.95968)[c] (11)	(41.01366)[c] (11)
	(63.49585)[d] (31)	(53.59660)[d] (11)	(39.94425)[d] (11)

[a]Shear correction factor $\kappa^2 = 1$.
[b]Shear correction factor $\kappa^2 = 0.86667$.
[c]Shear correction factor $\kappa^2 = 5/6$.
[d]Shear correction factor $\kappa^2 = \pi^2/12$.

where N_{x1} corresponds to $\tilde{N}_{cr}$ for the loading case $(\xi_1 = -1,\ \xi_2 = 0)$. Similarly, for plates subjected to monoaxial in-plane compressive applied load in the X_2-direction $(\xi_1 = 0,\ \xi_2 = -1)$, Eq. (29) reduces to

$$N_{x2} = -\frac{\theta\pi^2(m^2 + n^2\eta^2)^2}{(m^2\pi^2 + n^2\pi^2\eta^2 + \theta)n^2\eta^2}, \tag{31}$$

where N_{x2} corresponds to $\tilde{N}_{cr}$ for the loading case $(\xi_1 = 0,\ \xi_2 = -1)$. Upon assuming $\eta_2 = 1/\eta_1$, $\theta_2 = \theta_1/\eta_1^2$, $n_2 = m_1$ and $n_1 = m_2$, Eqs. (30) and (31) give

$$N_{x1} = \eta_1^2 N_{x2}, \tag{32}$$

where subscripts 1 and 2 are used to distinguish θ, m, n and η in Eq. (30) from those in Eq. (31). Consider now the dimensionless critical buckling loads listed in Table 4. It is seen that, for example, the (1,3) mode for $\eta_2 = 0.4$ and $\delta_2 = 0.2$ (with $N_{x2} = 32.26650$) listed for the loading case $(\xi_1 = 0,\ \xi_2 = -1)$ can be related to the (3,1) mode for $\eta_1 = 2.5$ and $\delta_1 = 0.08$ (with $N_{x1} = 201.66563$) given for the loading case $(\xi_1 = -1,\ \xi_2 = 0)$, through the relation Eq. (32). In fact, the S-S-S-S plate with aspect ratio η_1 and thickness ratio δ_1 and subjected to monoaxial in-plane compressive load in the X_1-direction can be considered as the S-S-S-S plate

with aspect ratio $\eta_2 = 1/\eta_1$ and thickness ratio $\delta_2 = \eta_1\delta_1$ which is subjected to monoaxial in-plane compressive load in the X_2-direction.

Consider now two S-S-S-S plates subjected to monoaxial in-plane compressive load in the X_1-direction. By using Eq. (30) one may write

$$\overset{*}{N}_{x1} = \frac{\overset{*}{\eta}_1^2}{\eta_1^2} N_{x1} \quad \text{if } \frac{\eta_1}{\overset{*}{\eta}_1} = \frac{m_1}{\overset{*}{m}_1} = \frac{\overset{*}{\delta}_1}{\delta_1}. \tag{33}$$

For example, the dimensionless critical buckling load $\overset{*}{N}_{x1} = 32.44143$ given in Table 4 for $\overset{*}{\eta}_1 = 1$ and $\overset{*}{\delta}_1 = 0.2$, may related to the dimensionless critical buckling load $N_{x1} = 129.76572$ listed for $\eta_1 = 2$ and $\delta_1 = 0.1$ through Eq. (33). In fact, at nodal equispaced lines there are the same conditions that on simply supported edges.

6. Conclusions

In this work the Mindlin plate theory is used to investigate the buckling behavior of moderately thick rectangular plates subjected to monoaxial in-plane compressive load in the X_1-direction ($\xi_1 = -1$, $\xi_2 = 0$), equal biaxial in-plane compressive load ($\xi_1 = -1$, $\xi_2 = -1$) and monoaxial in-plane compressive load in the X_2-direction ($\xi_1 = 0$, $\xi_2 = -1$). The exact closed-form buckling equations are derived for the six cases having two opposite sides simply supported. The six cases considered are namely S-S-S-S, S-C-S-S, S-C-S-C, S-S-S-F, S-F-S-F and S-C-S-F plates. The advantages of the proposed closed-form buckling equations are the following:

- They are capable of predicting with high accuracy the critical buckling load within the validity of the Mindlin plate theory since an exact analytical solution is used.
- They provide a closed-form buckling equation that can be easily solved numerically by designers and engineers.

The transverse deflection are also given in closed-form for all the six cases, and the buckled mode shapes can be easily plotted. Accurate dimensionless critical buckling loads are presented for different in-plane loading conditions, aspect ratios and thickness ratios; they can be used as a benchmark for numerical codes. The effects of boundary conditions, loading conditions, aspect ratios and thickness ratios are examined and discussed in detail. Finally, based on comparison with previously published results, the accuracy of the present results is shown.

Appendix A

In order to solve the three coupled partial differential Eqs. (8a–c), it is more convenient to deal with a single equation on the transverse deflection ψ_3. This can be obtained by differentiating Eqs. (8a) and (8b) with respect to X_1 and X_2, respectively, then multiplying the last one by η, summing them up and by using Eq. (8c), we obtain:

$$\begin{aligned} &a_1(\tilde{\psi}_{3,11} + \eta^2\tilde{\psi}_{3,22})_{,11} + a_2\eta^2(\tilde{\psi}_{3,11} + \eta^2\tilde{\psi}_{3,22})_{,22} + a_3(\tilde{\psi}_{3,11} + \eta^2\tilde{\psi}_{3,22}) \\ &\quad + a_4\tilde{\psi}_{3,11} + a_5\eta^2\tilde{\psi}_{3,22} + a_6\tilde{\psi}_3 = 0, \end{aligned} \tag{A.1}$$

where

$$a_1 = 1 + \frac{\tilde{N}_1}{\theta}, \quad a_2 = 1 + \frac{\tilde{N}_2}{\theta}, \quad a_3 = \frac{\beta^2}{\theta}, \tag{A.2–A.4}$$

$$a_4 = \frac{\beta^2\kappa^2\nu_1}{\theta} + \left(\frac{\beta^2\kappa^2\nu_1}{\theta^2} - 1\right)\tilde{N}_1, \quad a_5 = \frac{\beta^2\kappa^2\nu_1}{\theta} + \left(\frac{\beta^2\kappa^2\nu_1}{\theta^2} - 1\right)\tilde{N}_2, \tag{A.5,A.6}$$

$$a_6 = \left(\frac{\beta^2\kappa^2\nu_1}{\theta^2} - 1\right)\beta^2. \tag{A.7}$$

The solution of Eq. (A.1) may be assumed to be

$$\psi_3 = W_1 + W_2 = f_1(X_1)g_1(X_2) + f_2(X_1)g_2(X_2). \tag{A.8}$$

Substituting the above solution into Eq. (A.1) yields

$$a_1\frac{f_{1,1111}}{f_1} + (a_3+a_4)\frac{f_{1,11}}{f_1} + a_2\eta^4\frac{g_{1,2222}}{g_1} + (a_3+a_5)\eta^2\frac{g_{1,22}}{g_1} + (a_1+a_2)\eta^2\frac{f_{1,11}}{f_1 g_1}g_{1,22} + a_6 = 0, \tag{A.9}$$

$$a_1\frac{f_{2,1111}}{f_2} + (a_3+a_4)\frac{f_{2,11}}{f_2} + a_2\eta^4\frac{g_{2,2222}}{g_2} + (a_3+a_5)\eta^2\frac{g_{2,22}}{g_2} + (a_1+a_2)\eta^2\frac{f_{2,11}}{f_2 g_2}g_{2,22} + a_6 = 0. \tag{A.10}$$

Inspection of Eqs. (A.9) and (A.10) suggests that the functions $f_i(X_1)$ and $g_i(X_2)(i = 1,2)$ should be characterized by the equations

$$f_{i,11} = \pm\mu_i^2 f_i, \quad g_{i,22} = \pm\lambda_i^2 g_i, \tag{A.11,A.12}$$

where μ_i^2 and λ_i^2 are separation constants to be determined. It can be easily shown that the solutions of the equation $f_{i,11} = \mu_i^2 f_i$ are not suitable for satisfying the boundary conditions when two opposite edges at $X_1 = 0$ and 1 are simply supported. Hence, the following solutions to Eqs. (A.11) and (A.12) may be selected:

$$f_i(X_1) = \tilde{a}_i \sin\mu_i X_1 + \tilde{b}_i \cos\mu_i X_1, \tag{A.13}$$

$$g_i(X_2) = \tilde{c}_i \sin\lambda_i X_2 + \tilde{d}_i \cos\lambda_i X_2, \tag{A.14}$$

$$g_i(X_2) = c_i^* \sinh\lambda_i X_2 + d_i^* \cosh\lambda_i X_2. \tag{A.15}$$

As it was discussed in an earlier paper by Hosseini-Hashemi and Arsanjani [38], no loss of generality may arise due to selection of any possible set of solutions. As a result we carry on our derivation based on the set of selected solutions as

$$f_i(X_1) = \tilde{a}_i \sin\mu_i X_1 + \tilde{b}_i \cos\mu_i X_1, \tag{A.14′}$$

$$g_1(X_2) = \tilde{c}_1 \sin\lambda_1 X_2 + \tilde{d}_1 \cos\lambda_1 X_2, \tag{A.15′}$$

$$g_2(X_2) = c_2^* \sinh\lambda_2 X_2 + d_2^* \cosh\lambda_2 X_2, \tag{A.16′}$$

which in turn give

$$f_{i,11} = -\mu_i^2 f_i, \quad g_{1,22} = -\lambda_1^2 g_1, \quad g_{2,22} = \lambda_2^2 g_2. \tag{A.17–A.19}$$

It is also pertinent to mention that, since $W_1 = f_1(X_1)g_1(X_2)$ and $W_2 = f_2(X_1)g_2(X_2)$ satisfy Eqs. (9a) and (9b), respectively, the relationship between λ_i, μ_i and α_i for the set of selected solutions can be expressed as

$$\alpha_1^2 = \mu_1^2 + \eta^2\lambda_1^2, \quad \alpha_2^2 = \mu_2^2 - \eta^2\lambda_2^2. \tag{A.20,A.21}$$

Substituting now Eqs. (A.17)–(A.19) into Eqs. (A.9) and (A.10) gives

$$a_2\eta^4\lambda_1^4 + (a_1\mu_1^2 + a_2\mu_1^2 - a_3 - a_5)\eta^2\lambda_1^2 + a_1\mu_1^4 - (a_3+a_4)\mu_1^2 + a_6 = 0, \tag{A.22}$$

$$a_2\eta^4\lambda_2^4 - (a_1\mu_2^2 + a_2\mu_2^2 - a_3 - a_5)\eta^2\lambda_2^2 + a_1\mu_2^4 - (a_3+a_4)\mu_2^2 + a_6 = 0. \tag{A.23}$$

Thus, for simply supported edges at $X_1 = 0$ and $X_1 = 1$ ($\mu_1 = \mu_2 = \mu$) we may write:

$$\lambda_1^2 = \frac{-\lambda + \sqrt{\lambda^2 - 4\alpha}}{2}, \quad \lambda_2^2 = \frac{\lambda + \sqrt{\lambda^2 - 4\alpha}}{2}, \tag{A.24,A.25}$$

where

$$\lambda = \frac{a_1\mu^2 + a_2\mu^2 - a_3 - a_5}{a_2\eta^2}, \quad \alpha = \frac{a_1\mu^4 - (a_3 + a_4)\mu^2 + a_6}{a_2\eta^4}. \tag{A.26,A.27}$$

Substituting the expression of ψ_3 in Eq. (A.8) into Eq. (8c) yields

$$\tilde{\psi}_{1,1} + \eta\tilde{\psi}_{2,2} = (a_3 - a_1\mu^2 - a_2\eta^2\lambda_1^2)W_1 + (a_3 - a_1\mu^2 + a_2\eta^2\lambda_2^2)W_2, \tag{A.28}$$

assuming

$$\tilde{\psi}_1 = C_1 W_{1,1} + C_2 W_{2,1} - \eta W_{3,2}, \quad \tilde{\psi}_2 = C_1\eta W_{1,2} + C_2\eta W_{2,2} + W_{3,1}, \tag{A.29,A.30}$$

substituting in Eq. (A.28) gives

$$C_1 = \frac{a_1\mu^2 + a_2\eta^2\lambda_1^2 - a_3}{\alpha_1^2}, \quad C_2 = \frac{a_1\mu^2 - a_2\eta^2\lambda_2^2 - a_3}{\alpha_2^2}. \tag{A.31,A.32}$$

In view of Eqs. (A.8), (A.29) and (A.30), Eqs. (8a) and (8b) may be written as

$$\left(C_1\alpha_3^2 + \frac{\theta}{\nu_1} - C_1\frac{\alpha_1^2}{\nu_1}\right)W_{1,1} + \left(C_2\alpha_3^2 + \frac{\theta}{\nu_1} - C_2\frac{\alpha_2^2}{\nu_1}\right)W_{2,1} - \eta(W_{3,11} + \eta^2 W_{3,22} + \alpha_3^2 W_3)_{,2} = 0, \tag{A.33}$$

$$\eta\left(C_1\alpha_3^2 + \frac{\theta}{\nu_1} - C_1\frac{\alpha_1^2}{\nu_1}\right)W_{1,2} + \eta\left(C_2\alpha_3^2 + \frac{\theta}{\nu_1} - C_2\frac{\alpha_2^2}{\nu_1}\right)W_{2,2} + (W_{3,11} + \eta^2 W_{3,22} + \alpha_3^2 W_3)_{,1} = 0, \tag{A.34}$$

where

$$\alpha_3^2 = \frac{\kappa^2\beta^2}{\theta} - \frac{\theta}{\nu_1}. \tag{A.35}$$

To satisfy Eqs. (A.33) and (A.34) we can write

$$C_1 = \frac{\theta}{\alpha_1^2 - \nu_1\alpha_3^2}, \quad C_2 = \frac{\theta}{\alpha_2^2 - \nu_1\alpha_3^2}, \tag{A.36,A.37}$$

$$W_{3,11} + \eta^2 W_{3,22} = -\alpha_3^2 W_3. \tag{A.38}$$

Upon assuming $W_3 = f_3(X_1)g_3(X_2)$, Eq. (A.38) may be separated into

$$f_{3,11} = -\mu_3^2 f_3, \quad g_{3,22} = \pm\lambda_3^2 g_3, \tag{A.39,A.40}$$

where

$$\alpha_3^2 = \mu_3^2 \pm \eta^2\lambda_3^2. \tag{A.41}$$

Once again it should be emphasized that, as a result of having simply supported edges at $X_1 = 0$ and 1, a solution based on $f_{3,11} = \mu_3^2 f_3$ is irrelevant and ($\mu_1 = \mu_2 = \mu_3 = \mu$). Thus, there are two possible solutions for $g_3(X_2)$ as

$$g_3(X_2) = \tilde{c}_3 \sin\lambda_3 X_2 + \tilde{d}_3 \cos\lambda_3 X_2 \text{ or } g_3(X_2) = c_3^* \sinh\lambda_3 X_2 + d_3^* \cosh\lambda_3 X_2 \tag{A.42,A.43}$$

and no loss of generality may arise due to the selection of either of the two solutions.

Appendix B. Different possible solution for Eqs. (13a–c)

In order to solve Eqs. (13a–c), the method of separation of variables may be used. Assuming $W_i = f_i(X_1)g_i(X_2)$ ($i = 1,2,3$) we obtain

$$f_{i,11} = \pm\mu_i^2 f_i, \quad g_{i,22} = \pm\lambda_i^2 g_i, \tag{B.1,B.2}$$

where μ_i^2 and λ_i^2 are separation constants. It can be easily shown that by examining the boundary conditions, a solution to the equations $f_{i,11} = \mu_i^2 f_i$ are not suitable for satisfying the boundary conditions when two

opposite edges at $X_1 = 0$ and 1 are simply supported. Hence, the following solutions to Eqs. (B.1) and (B.2) may be selected

$$f_i(X_1) = \tilde{a}_i \sin(\mu_i X_1) + \tilde{b}_i \cos(\mu_i X_1), \tag{B.3}$$

$$g_i(X_2) = \tilde{c}_i \sin(\lambda_i X_2) + \tilde{d}_i \cos(\lambda_i X_2), \tag{B.4}$$

$$g_i(X_2) = c_i^* \sinh(\lambda_i X_2) + d_i^* \cosh(\lambda_i X_2). \tag{B.5}$$

Assuming $\alpha_1 > \mu_1$, $\alpha_2 > \mu_2$ and $\alpha_3 > \mu_3$, one set of solutions may be expressed as

$$W_1 = [A_1 \sin(\lambda_1 X_2) + A_2 \cos(\lambda_1 X_2)]\sin(\mu_1 X_1) + [B_1 \sin(\lambda_1 X_2) + B_2 \cos(\lambda_1 X_2)]\cos(\mu_1 X_1), \tag{B.6}$$

$$W_2 = [A_3 \sin(\lambda_2 X_2) + A_4 \cos(\lambda_2 X_2)]\sin(\mu_2 X_1) + [B_3 \sin(\lambda_2 X_2) + B_4 \cos(\lambda_2 X_2)]\cos(\mu_2 X_1), \tag{B.7}$$

$$W_3 = [A_5 \sin(\lambda_3 X_2) + A_6 \cos(\lambda_3 X_2)]\cos(\mu_3 X_1) + [B_5 \sin(\lambda_3 X_2) + B_6 \cos(\lambda_3 X_2)]\sin(\mu_3 X_1), \tag{B.8}$$

where

$$\alpha_1^2 = \mu_1^2 + \eta^2 \lambda_1^2, \quad \alpha_2^2 = \mu_2^2 + \eta^2 \lambda_2^2, \quad \alpha_3^2 = \mu_3^2 + \eta^2 \lambda_3^2. \tag{B.9–B.11}$$

The next three sets of solutions may be written as

$$W_1 = [A_1 \sin(\lambda_1 X_2) + A_2 \cos(\lambda_1 X_2)]\sin(\mu_1 X_1) + [B_1 \sin(\lambda_1 X_2) + B_2 \cos(\lambda_1 X_2)]\cos(\mu_1 X_1), \tag{B.12}$$

$$W_2 = [A_3 \sin(\lambda_2 X_2) + A_4 \cos(\lambda_2 X_2)]\sin(\mu_2 X_1) + [B_3 \sin(\lambda_2 X_2) + B_4 \cos(\lambda_2 X_2)]\cos(\mu_2 X_1), \tag{B.13}$$

$$W_3 = [A_5 \sinh(\lambda_3 X_2) + A_6 \cosh(\lambda_3 X_2)]\cos(\mu_3 X_1) + [B_5 \sinh(\lambda_3 X_2) + B_6 \cosh(\lambda_3 X_2)]\sin(\mu_3 X_1), \tag{B.14}$$

where

$$\alpha_1 > \mu_1, \quad \alpha_2 > \mu_2, \quad \alpha_3 < \mu_3, \tag{B.15–B.17}$$

$$\alpha_1^2 = \mu_1^2 + \eta^2 \lambda_1^2, \quad \alpha_2^2 = \mu_2^2 + \eta^2 \lambda_2^2, \quad \alpha_3^2 = \mu_3^2 - \eta^2 \lambda_3^2, \tag{B.18–B.20}$$

$$W_1 = [A_1 \sin(\lambda_1 X_2) + A_2 \cos(\lambda_1 X_2)]\sin(\mu_1 X_1) + [B_1 \sin(\lambda_1 X_2) + B_2 \cos(\lambda_1 X_2)]\cos(\mu_1 X_1), \tag{B.21}$$

$$W_2 = [A_3 \sinh(\lambda_2 X_2) + A_4 \cosh(\lambda_2 X_2)]\sin(\mu_2 X_1) + [B_3 \sinh(\lambda_2 X_2) + B_4 \cosh(\lambda_2 X_2)]\cos(\mu_2 X_1), \tag{B.22}$$

$$W_3 = [A_5 \sin(\lambda_3 X_2) + A_6 \cos(\lambda_3 X_2)]\cos(\mu_3 X_1) + [B_5 \sin(\lambda_3 X_2) + B_6 \cos(\lambda_3 X_2)]\sin(\mu_3 X_1), \tag{B.23}$$

where

$$\alpha_1 > \mu_1, \quad \alpha_2 < \mu_2, \quad \alpha_3 > \mu_3, \tag{B.24–B.26}$$

$$\alpha_1^2 = \mu_1^2 + \eta^2 \lambda_1^2, \quad \alpha_2^2 = \mu_2^2 - \eta^2 \lambda_2^2, \quad \alpha_3^2 = \mu_3^2 + \eta^2 \lambda_3^2, \tag{B.27–B.29}$$

and

$$W_1 = [A_1 \sin(\lambda_1 X_2) + A_2 \cos(\lambda_1 X_2)]\sin(\mu_1 X_1) + [B_1 \sin(\lambda_1 X_2) + B_2 \cos(\lambda_1 X_2)]\cos(\mu_1 X_1), \tag{B.30}$$

$$W_2 = [A_3\sinh(\lambda_2 X_2) + A_4\cosh(\lambda_2 X_2)]\sin(\mu_2 X_1) + [B_3\sinh(\lambda_2 X_2) + B_4\cosh(\lambda_2 X_2)]\cos(\mu_2 X_1), \tag{B.31}$$

$$W_3 = [A_5\sinh(\lambda_3 X_2) + A_6\cosh(\lambda_3 X_2)]\cos(\mu_3 X_1) + [B_5\sinh(\lambda_3 X_2) + B_6\cosh(\lambda_3 X_2)]\sin(\mu_3 X_1), \tag{B.32}$$

where

$$\alpha_1 > \mu_1, \quad \alpha_2 < \mu_2, \quad \alpha_3 < \mu_3, \tag{B.33–B.35}$$

$$\alpha_1^2 = \mu_1^2 + \eta^2\lambda_1^2, \quad \alpha_2^2 = \mu_2^2 - \eta^2\lambda_2^2, \quad \alpha_3^2 = \mu_3^2 - \eta^2\lambda_3^2. \tag{B.36–B.38}$$

To satisfy the boundary conditions when two opposite edges at $X_1 = 0$ and 1 are simply supported, we should write:

$$\mu_1 = \mu_2 = \mu_3 = m\pi, \quad B_1 = B_2 = B_3 = B_4 = B_5 = B_6 = 0. \tag{B.39,B.40}$$

The discussion on the existence of eigenvalues such that $\alpha_1 < \mu_1$ is presented in Ref. [38]. Anyway, it is not difficult to show that $\alpha_3 > \alpha_2$ by rewriting Eq. (16c) as

$$\frac{\alpha_3^2}{\alpha_2^2} = \frac{12\kappa^2}{\beta^2\delta^2}\alpha_1^2, \tag{B.41}$$

where the right-hand side of Eq. (B.41) is always greater than one. Thus, the set of solutions given by Eqs. (B.12)–(B.14) must be eliminated to satisfy (B.15)–(B.17). Close examination of Eq. (16c) in case of $\beta = 0$ (the critical buckling load parameter $\tilde{N}_{cr}$ may be determined by setting $\beta = 0$ in the corresponding characteristic equation of each individual case) reveals that $\alpha_3^2 < 0$. Thus, there will exist one sets of solution, given by Eqs. (B.30)–(B.32) which is able to satisfy the conditions (B.33)–(B.38).

Appendix C. Nondimensional transverse deflection

In order to find the nondimensional transverse deflection ($\tilde{U}_3 = \tilde{\psi}_3$), the previously mentioned procedure for the determination of characteristic equations for the six cases may be applied. Focusing on the arbitrary constants A_i and presenting them in terms of A_1, leads to the following expressions of the nondimensional transverse displacement for the six different boundary conditions.

S-S-S-S case:

$$\tilde{U}_3 = A_1\sin(\lambda_1 X_2)\sin(m\pi X_1). \tag{C.1}$$

S-C-S-S case:

$$\tilde{U}_3 = A_1\left[\sin(\lambda_1 X_2) - \frac{\sin\lambda_1}{\sinh\lambda_2}\sinh(\lambda_2 X_2)\right]\sin(m\pi X_1). \tag{C.2}$$

S-C-S-C case:

$$\tilde{U}_3 = A_1[\sin(\lambda_1 X_2) + b_1\cos(\lambda_1 X_2) - (b_1\cos\lambda_1 - b_1\cosh\lambda_2 + \sin\lambda_1)\frac{\sinh(\lambda_2 X_2)}{\sinh\lambda_2} - b_1\cosh(\lambda_2 X_2)]\sin(m\pi X_1), \tag{C.3}$$

where

$$b_1 = -\frac{\eta^2\lambda_3(C_2\lambda_2\sin\lambda_1 - C_1\lambda_1\sinh\lambda_2)\sinh\lambda_3 + (C_1 - C_2)\mu^2\sin\lambda_1\sinh\lambda_2}{C_2\eta^2\lambda_2\lambda_3(\cos\lambda_1 - \cosh\lambda_2)\sinh\lambda_3 + (C_1 - C_2)\mu^2(\cos\lambda_1 - \cosh\lambda_3)\sinh\lambda_2}. \tag{C.4}$$

S-S-S-F case:

$$\tilde{U}_3 = A_1\{[\sin(\lambda_1 X_2) + b_2\cos(\lambda_1 X_2)]\cosh\lambda_2 + \frac{L_1\lambda_1}{L_3\lambda_2}\sinh[\lambda_2(1 - X_2)] - (b_2\cos\lambda_1 + \sin\lambda_1)\cosh(\lambda_2 X_2)\}\frac{\sin(m\pi X_1)}{\cosh\lambda_2}, \tag{C.5}$$

where

$$b_2 = -\frac{R_1}{R_2}, \tag{C.6}$$

$$R_1 = C_2L_2(L_3\lambda_2 \sin\lambda_1 - L_1\lambda_1 \sinh\lambda_2)\cosh\lambda_3 + (C_1 - C_2)\lambda_2\mu^2(1-\nu)(L_3 \sin\lambda_1 + 2\eta^2\lambda_1\lambda_3 \sinh\lambda_3)\cosh\lambda_2, \tag{C.7}$$

$$R_2 = L_3\lambda_2\{C_2L_2 \cos\lambda_1 \cosh\lambda_3 + [(C_1 - C_2)\mu^2(1-\nu)\cos\lambda_1 + C_1L_4 \cosh\lambda_3]\cosh\lambda_2\}. \tag{C.8}$$

S-F-S-F case:

$$\tilde{U}_3 = A_1[\sin(\lambda_1X_2) + b_3\cos(\lambda_1X_2) - \frac{L_1\lambda_1}{L_3\lambda_2}\sinh(\lambda_2X_2) + b_4\cosh(\lambda_2X_2)]\sin(m\pi X_1), \tag{C.9}$$

where

$$b_3 = -\frac{R_3}{R_4}, \quad b_4 = \frac{R_5}{R_6}, \tag{C.10}$$

$$R_3 = 2(C_1 - C_2)\eta^2\mu^2\lambda_1\lambda_2\lambda_3(1-\nu)(\cos\lambda_1 - \cosh\lambda_3)\sinh\lambda_2 - C_2L_1L_2\lambda_1(\cos\lambda_1 - \cosh\lambda_2)\sinh\lambda_3, \tag{C.11}$$

$$R_4 = C_2L_1L_2\lambda_1 \sin\lambda_1 \sinh\lambda_3 - \lambda_2[2(C_1 - C_2)\eta^2\mu^2\lambda_1\lambda_3(1-\nu)\sin\lambda_1 + C_1L_3L_4 \sinh\lambda_3]\sinh\lambda_2, \tag{C.12}$$

$$R_5 = \eta^2\lambda_1\lambda_3(1-\nu)[(C_2 - 1)L_1(\cosh\lambda_2 - \cosh\lambda_3) + (C_1 - 1)L_3(b_3 \sin\lambda_1 - \cos\lambda_1 + \cosh\lambda_3)] - b_3C_1L_3L_4 \sinh\lambda_3, \tag{C.13}$$

$$R_6 = L_3[(C_2 - 1)\eta^2\lambda_2\lambda_3(1-\nu)\sinh\lambda_2 - C_2L_2 \sinh\lambda_3]. \tag{C.14}$$

S-C-S-F case:

$$\tilde{U}_3 = A_1\{[\sin(\lambda_1X_2) + b_5\cos(\lambda_1X_2)]\cosh\lambda_2 + \frac{L_1\lambda_1}{L_3\lambda_2}\sinh[\lambda_2(1 - X_2)] - (b_5\cos\lambda_1 + \sin\lambda_1)\cosh(\lambda_2X_2)\}\frac{\sin(m\pi X_1)}{\cosh\lambda_2}, \tag{C.15}$$

where

$$b_5 = -\frac{R_7}{R_8}, \tag{C.16}$$

$$R_7 = C_2L_2(L_3\lambda_2 \sin\lambda_1 - L_1\lambda_1 \sinh\lambda_2)\cosh\lambda_3 + (C_1 - C_2)\mu^2\lambda_2(1-\nu)(L_3 \sin\lambda_1 + 2\eta^2\lambda_1\lambda_3 \sinh\lambda_3)\cosh\lambda_2, \tag{C.17}$$

$$R_8 = L_3\lambda_2[(C_1 - C_2)\mu^2(1-\nu)\cos\lambda_1 \cosh\lambda_2 + (C_2L_2 \cos\lambda_1 + C_1L_4 \cosh\lambda_2)\cosh\lambda_3]. \tag{C.18}$$

References

[1] M. Amabili, *Nonlinear Vibrations and Stability of Shells and Plates*, Cambridge University Press, New York, USA, 2008.

[2] J.N. Reddy, A general non-linear third-order theory of plates with moderate thickness, *International Journal of Non-Linear Mechanics* 25 (1990) 677–686.

[3] P.S. Bulson, *The Stability of Flat Plates*, Chatto and Windus, London, 1970.

[4] H. Kobayashi, K. Sonoda, Buckling of rectangular plates with tapered thickness, *Journal of Structural Engineering* 116 (1990) 1278–1289.

[5] H. Kobayashi, K. Sonoda, Vibration and buckling of tapered rectangular plates with two opposite edges simply supported and the other two edges elastically restrained against rotation, *Journal of Sound and Vibration* 146 (1991) 323–337.
[6] A. Leissa, Advances and trends in plate buckling research, Research in structural and solid mechanics, NASA CP-2245, 1982.
[7] S. Srinivas, Buckling of thick rectangular plates, *AIAA Journal* 7 (1969) 1645–1648.
[8] E.J. Brunelle, Buckling of transversely isotropic Mindlin plates, *AIAA Journal* 19 (1971) 1018–1022.
[9] E.J. Brunelle, S.R. Robertson, Initially stressed Mindlin plates, *AIAA Journal* 12 (1974) 1036–1045.
[10] G.V. Rao, J. Venkataramana, K. Kanaka Raju, Stability of moderately thick rectangular plates using a high precision triangular element, *Computers and Structures* 5 (1975) 257–260.
[11] J.-W. Luo, A hybrid/mixed model finite element analysis for buckling of moderately thick plates, *Computers and Structures* 15 (1982) 359–364.
[12] T. Sakiyama, H. Matsuda, Elastic buckling of rectangular Mindlin plate with mixed boundary conditions, *Computers and Structures* 25 (1987) 801–808.
[13] C.M. Wang, Allowance for prebuckling deformations in buckling load relationship between Mindlin and Kirchhoff simply supported plates of general polygonal shape, *Engineering Structures* 17 (1995) 413–418.
[14] C.M. Wang, J.N. Reddy, Buckling load relationship between Reddy and Kirchhoff plates of polygonal shape with simply supported edges, *Mechanics Research Communications* 24 (1997) 103–105.
[15] A.W. Leissa, J.-H. Kang, Exact solutions for vibration and buckling of an SS-C-SS-C rectangular plate loaded by linearly varying \in-plane stresses, *International Journal of Mechanical Sciences* 44 (2002) 1925–1945.
[16] J.-H. Kang, A.W. Leissa, Vibration and buckling of SS-F-SS-F rectangular plates loaded by in-plane moments, *International Journal of Stability and Dynamics* 1 (2001) 527–543.
[17] J.H. Kang, A.W. Leissa, Exact solutions for the buckling of rectangular plates having linearly varying in-plane loading on two opposite simply supported edges, *International Journal of Solids and Structures* 42 (2005) 4220–4238.
[18] J.N. Reddy, N.D. Phan, Stability and vibration of isotropic, orthotropic and laminated plates according to a higher-order shear deformation theory, *Journal of Sound and Vibration* 98 (1985) 157–170.
[19] K.M. Liew, Y. Xiang, S. Kittipornchai, Analytical buckling solutions for Mindlin plates involving free edges, *International Journal of Mechanical Sciences* 38 (10) (1996) 1127–1138.
[20] C.M. Wang, Y. Xiang, S. Kitipornchai, K.M. Liew, Buckling solutions for Mindlin plates of various shapes, *Engineering Structures* 16 (1994) 119–127.
[21] K.M. Liew, J.-B. Han, Z.M. Xiao, H. Du, Differential quadrature method for Mindlin plates on Winkler foundations, *International Journal of Mechanical Sciences* 38 (1996) 405–421.
[22] H.-S. Shen, Postbuckling of Reissner–Mindlin plates under biaxial compression and lateral pressure and resting on elastic foundations, *Computer Methods in Applied Mechanics and Engineering* 173 (1999) 135–146.
[23] H.-S. Shen, Postbuckling of free edge Reissner–Mindlin Plates elastically supported on a two-parameter foundation and subjected to biaxial compression and transverse loads, *Engineering Structures* 23 (2001) 260–270.
[24] T. Mizusawa, Buckling of rectangular Mindlin plates with tapered thickness by the spline strip method, *International Journal of Solids and Structures* 30 (1993) 1663–1677.
[25] K.Y. Lam, C.M. Wang, X.Q. He, Canonical exact solutions for Levy-plates on two-parameter foundation using Green's functions, *Engineering Structures* 22 (2000) 364–378.
[26] L.X. Penga, K.M. Liew, S. Kitipornchai, Buckling and free vibration analyses of stiffened plates using the FSDT mesh-free method, *Journal of Sound and Vibration* 289 (2006) 421–449.
[27] Y. Xiang, G.W. Wei, Exact solutions for buckling and vibration of stepped rectangular Mindlin plates, *International Journal of Solids and Structures* 41 (2004) 279–294.
[28] D.J. Dawe, O.L. Roupaeil, Buckling of rectangular Mindlin plates, *Computers and Structures* 15 (1982) 461–471.
[29] Y. Xiang, Numerical Developments in Solving the Buckling and Vibration of Mindlin Plates, PhD Thesis, The University of Queensland, Australia, 1993.
[30] S. Kitipornchai, Y. Xiang, C.M. Wang, K.M. Liew, Buckling of thick skew plates, *International Journal for Numerical Methods in Engineering* 36 (1993) 1299–1310.
[31] Y. Xiang, C.M. Wang, S. Kitipornchai, Buckling of skew Mindlin plates subjected to in-plane shear loadings, *International Journal of Mechanical Science* 37 (1995) 1089–1101.
[32] Y. Xiang, C.M. Wang, S. Kitipornchai, Exact vibration solution for initially stressed Mindlin plates on Pasternak foundations, *International Journal of Mechanical Science* 36 (1994) 311–316.
[33] C.M. Wang, K.M. Liew, Y. Xiang, S. Kitipornchai, Buckling of rectangular Mindlin plates with internal line supports, *International Journal of Solids and Structures* 30 (1993) l–17.
[34] K.M. Liew, X.L. Chen, Buckling of rectangular Mindlin plates subjected to partial in-plane edge loads using the radial point interpolation method, *International Journal of Solids and Structures* 41 (2004) 1677–1695.
[35] I. Shufrin, M. Eisenberger, Stability and vibration of shear deformable plates—first order and higher order analyses, *International Journal of Solids and Structures* 42 (2005) 1225–1251.
[36] F.-L. Liu, Differential quadrature element method for buckling analysis of rectangular Mindlin plates having discontinuities, *International Journal of Solids and Structures* 38 (2001) 2305–2321.
[37] A.W. Leissa, Vibration of plates, NASA, SP-160, 1969.
[38] S. Hosseini-Hashemi, M. Arsanjani, Exact characteristic equations for some of classical boundary conditions of vibrating moderately thick rectangular plates, *International Journal of Solids and Structures* 42 (2005) 819–853.